

Considerations in optimizing CMB polarization experiments to constrain inflationary physics

Licia Verde^{1*}, Hiranya V. Peiris^{2†} and Raul Jimenez^{1‡}

¹*Dept. of Physics and Astronomy, University of Pennsylvania, 209 South 33rd Street, Philadelphia, PA-19104, USA.*

²*Kavli Institute for Cosmological Physics and Enrico Fermi Institute, University of Chicago, Chicago IL 60637, USA.*

7 September 2018

ABSTRACT

We quantify the limiting factors in optimizing current-technology cosmic microwave background (CMB) polarization experiments to learn about inflationary physics. We consider space-based, balloon-borne and ground-based experiments. We find that foreground contamination and residuals from foreground subtraction are ultimately the limiting factors in detecting a primordial gravity wave signal. For full-sky space-based experiments, these factors hinder the detection of tensor-to-scalar ratios of $r < 10^{-3}$ on large scales, while for ground-based experiments these factors impede the ability to apply delensing techniques. We consider ground-based/balloon-borne experiments of currently planned or proposed designs and find that it is possible for a value of $r = 0.01$ to be measured at $\sim 3\text{-}\sigma$ level. A small space-based CMB polarization experiment, with current detector technology and full sky coverage, can detect $r \sim 1 \times 10^{-3}$ at the $\sim 3\text{-}\sigma$ level, but a markedly improved knowledge of polarized foregrounds is needed. We advocate using as wide a frequency coverage as possible in order to carry out foreground subtraction at the percent level, which is necessary to measure such a small primordial tensor amplitude.

To produce a clearly detectable ($>3\text{-}\sigma$) tensor component in a realistic CMB experiment, inflation must either involve large-field variations, $\Delta\phi \gtrsim 1$ or multi-field/hybrid models. Hybrid models can be easily distinguished from large-field models due to their blue scalar spectral index. Therefore, an observation of a tensor/scalar ratio and $n < 1$ in future experiments with the characteristics considered here may be an indication that inflation is being driven by some physics in which the inflaton cannot be described as a fundamental field.

Key words: cosmology: cosmic microwave background — cosmology: theory — cosmology: early universe

1 INTRODUCTION

The inflationary paradigm, proposed and elucidated by Guth (1981); Linde (1982); Albrecht & Steinhardt (1982); Sato (1981); Mukhanov & Chibisov (1981); Hawking (1982); Guth & Pi (1982); Starobinsky (1982); Bardeen et al. (1983); Mukhanov et al. (1992) has enjoyed resounding success in the current era of precision cosmology. Not only has its broad-brush prediction of a flat universe been successful, but the more detailed predictions of the simplest inflationary models, of Gaussian, adiabatic, and nearly (but not exactly) scale-invariant perturbations, are also perfectly

consistent with the data. Observations of the cosmic microwave background (CMB), in particular by the WMAP satellite (see Bennett et al. (2003a) and references therein), have been instrumental in these observational tests of inflation (Peiris et al. 2003; Barger et al. 2003; Leach & Liddle 2003; Kinney et al. 2004). Particularly exciting is WMAP’s detection of an anti-correlation between CMB temperature and polarization fluctuations at angular separations $\theta > 2^\circ$ (corresponding to the TE anti-correlation seen on scales $\ell \sim 100 - 150$), a distinctive signature of adiabatic fluctuations on super-horizon scales at the epoch of decoupling (Spergel & Zaldarriaga 1997), confirming a fundamental prediction of the inflationary paradigm. This is probably the least ambiguous signature of the acausal physics which characterize inflation, unlike the large-angle correlations in the CMB temperature which are contaminated by

* lverde@physics.upenn.edu

† Hubble Fellow, hiranya@cfcp.uchicago.edu

‡ raulj@physics.upenn.edu

“foregrounds” such as the Integrated Sachs-Wolfe (ISW) effect.

The detection and measurement of a stochastic gravitational-wave background would provide the next important key test of inflation. The CMB polarization anisotropy has the potential to reveal the signature of primordial gravity waves (Zaldarriaga & Seljak 1997; Kamionkowski et al. 1997); unlike the CMB temperature anisotropy, it can discriminate between contributions from density perturbations (a scalar quantity) and gravity waves (a tensor quantity). The polarization anisotropy can be decomposed into two orthogonal modes: E -mode polarization is the curl-free component, generated by both density and gravity-wave perturbations, and B -mode polarization is the divergence-free mode, which can only, to leading order, be produced by gravity waves. The primordial B -mode signal appears at large angular scales. On smaller scales, another effect, which is sub-dominant on large scales, kicks in and eventually dominates: weak gravitational lensing of the E -mode converts it into B -mode polarization (Zaldarriaga & Seljak 1998). These considerations motivate the current observational and experimental effort, such as on-going ground-based experiments (e.g. QUaD¹ (Church et al. 2003), CLOVER², PolarBeaR³, QUIET⁴) and planned or proposed space-based and balloon-borne missions (e.g. Planck⁵, SPIDER⁶, EBEX⁷ (Oxley et al. 2005), CMBPol⁸).

The primordial B -mode anisotropy, if it exists, is at least an order of magnitude smaller than the E -mode polarization. This, combined with the difficulty of separating primordial B -modes from lensing B -modes as well as polarized Galactic foregrounds, makes the measurement of a potentially-existing primordial gravity wave background a great experimental challenge. At the same time, as it is the “smoking gun” of inflation, the primordial B -mode detection and measurement can be regarded as the “holy grail” of CMB measurements.

There are five main obstacles to making a measurement of the primordial B -mode polarization, some being fundamental, and others being practical complications. The fundamental complications are: (i) the level of the primordial signal is not guided at present by theory: there are inflationary models consistent with the current CMB data which predict significant levels of primordial gravity waves, as well as models which predict negligible levels; (ii) the signal is not significantly contaminated by lensing only on the largest scales $\ell \lesssim \text{few} \times 10$ where cosmic variance is important; (iii) polarized foreground emission (mostly from our galaxy but also from extra-galactic sources) on these scales is likely to dominate the signal at all frequencies. Practical complications are: (iv) for the signal to be detected in a reasonable

time-scale, the instrumental noise needs to be reduced well below the photon noise limit for a single detector, so multiple detectors need to be used; (v) polarized foregrounds are not yet well known, and since any detection relies on foreground subtraction, foreground uncertainties may seriously compromise the goal.

Tucci et al. (2004) consider different foreground subtraction techniques and compute the minimum detectable r for future CMB experiments for no lensing contamination. Hirata & Seljak (2003) and Seljak & Hirata (2004) show how the lensing B -mode contamination can be subtracted out in the absence of foregrounds. Calculations of the minimum detectable primordial gravity wave signature on the CMB polarization data and related constraints on the inflationary paradigm have been discussed in the literature [e.g. Knox & Song (2002); Song & Knox (2003); Kinney (2003); Sigurdson & Cooray (2005)].

Bowden et al. (2004) discuss the optimization of a ground-based experiment (in particular, focusing on QUaD) and Hu et al. (2003) discuss the instrumental effects that can contaminate the detection.

In this work, we take a complementary approach. We first attempt to forecast the performance of realistic CMB experiments: space-based, balloon-borne and ground based; considering the covariance between cosmological parameters and primordial parameters, effects of foreground contamination, instrumental noise and the effect of partial sky coverage for ground-based experiments, and then consider what these realistic forecasts can teach us about inflation.

Given the recent advances in the knowledge of the polarized foregrounds (Leitch et al. 2005; Benoît et al. 2004) and in detector technology, we then attempt here to answer the following questions: How much can we learn about the physics of the early universe (i.e. can we test the inflationary paradigm and constrain inflationary models) from a realistic CMB experiment? At what point does instrumental noise and uncertainties in the foregrounds degrade the results that could be obtained from an ideal experiment (no noise, no foregrounds)? What will be the limiting factor: foreground subtraction or instrumental noise? How much can be learned from a full-sky space-based experiment vs. a partial-sky ground-based one? And finally: Given the large costs involved in improving the experiment (reducing noise by increasing the number of detectors and improving foreground cleaning by increasing the number of frequency channels), what is the point of diminishing returns?

We start in § 2 by reviewing recent literature on B -modes and inflationary physics, and summarizing present-day constraints on inflationary models. We describe our forecast method in § 3 and § 4. In § 5 we report the expected constraints on primordial parameters from a suite of experiments including instrumental noise and a realistic estimate of foregrounds. These results give us some guidance in optimizing future CMB polarization experiments for BB detection and for studying inflationary physics, which we report in § 6. In § 6 we also draw some conclusions on the constraints that can be applied to inflationary models based on the capabilities of these experiments.

¹ QUaD: http://www.stanford.edu/group/quest_telescope/

² CLOVER: <http://www.mrao.cam.ac.uk/~act21/clover.html>

³ PolarBeaR: <http://bolo.berkeley.edu/polarbear/index.html>

⁴ QUIET:

<http://cfcp.uchicago.edu/~peterh/polarimetry/quiet3.html>

⁵ Planck:

<http://sci.esa.int/science-e/www/area/index.cfm?fareaid=17>

⁶ SPIDER: http://www.astro.caltech.edu/~lgg/spider_front.htm

⁷ EBEX: <http://groups.physics.umn.edu/cosmology/ebex/>

⁸ CMBPol: <http://universe.nasa.gov/program/inflation.html>

2 B-MODES AND INFLATION

As Peiris et al. (2003) and Kinney et al. (2004) demonstrate, a wide class of phenomenological inflation models are compatible with the current CMB data. In the absence of specific knowledge of the fundamental physics underlying inflation, an important consideration is therefore to see what general statements one can make about inflation from various types of measurements. It is well-known (e.g. Liddle & Lyth (1993); Copeland et al. (1993b,a); Liddle (1994)) that a measurement of the amplitude of the tensor modes immediately fixes the value of the Hubble parameter H during inflation when the relevant scales are leaving the horizon, or equivalently, the potential of the scalar field driving inflation (the *inflaton*) and its first derivative, V and V' . The relations between these quantities are given by (see e.g. Lyth (1984))

$$H \equiv \dot{a}/a \simeq \frac{1}{M_{\text{Pl}}} \sqrt{\frac{V}{3}}, \quad (1)$$

$$r = \frac{2V}{3\pi^2 M_{\text{Pl}}^4 \Delta_{\mathcal{R}}^2(k_0)} \quad (2)$$

$$\begin{aligned} &\simeq \frac{2V}{3\pi^2 M_{\text{Pl}}^4} \frac{1}{2.95 \times 10^{-9} A(k_0)} \\ &= 8M_{\text{Pl}}^2 \left(\frac{V'}{V}\right)^2, \end{aligned} \quad (3)$$

where $M_{\text{Pl}} \equiv (8\pi G)^{-1/2} = m_{\text{pl}}/\sqrt{8\pi} = 2.4 \times 10^{18}$ GeV is the reduced Planck energy, $r = \Delta_h^2(k_0)/\Delta_{\mathcal{R}}^2(k_0)$ and Δ_h^2 and $\Delta_{\mathcal{R}}^2$ are the power spectra of the primordial tensor and curvature perturbations defined at the fiducial wavenumber $k_0 = 0.002 \text{ Mpc}^{-1}$, where the scalar amplitude $A(k_0)$ is also defined, following the notational convention of (Peiris et al. 2003).

A measurement of the spectral index of the scalar (density) perturbations fixes V'' , and a potential measurement of the running of the scalar spectral index carries information about the third derivative of the potential, V''' . Further, combining a measurement of the spectral index of tensor perturbations, n_t , with the tensor-to-scalar ratio r allows one to test the *inflationary consistency condition*, $r = -n_t/8$, that single-field slow roll models must satisfy. However, a precise determination of the tensor spectral index is likely to be even more difficult than a measurement of the tensor amplitude.

The current constraint on the tensor-to-scalar ratio at 95% significance from WMAP data alone gives the energy scale of slow-roll inflation as (Peiris et al. 2003):

$$V^{1/4} \leq 3.3 \times 10^{16} r^{1/4} \text{ GeV}; \quad (4)$$

This is the familiar result that a significant contribution of tensor modes to the CMB requires that inflation takes places at a high energy scale. If instead of using CMB only data we use the most stringent constraints to date on r , a 95% upper limit of $r < 0.36$, obtained from a compilation of current CMB plus large scale structure data (Seljak et al. 2004), one obtains

$$V^{1/4} \leq 2.6 \times 10^{16} \text{ GeV}, \quad (5)$$

or equivalently, $V^{1/4} \leq 2.2 \times 10^{-3} m_{\text{Pl}}$. Several authors (e.g.

Lyth (1997); Kinney (2003)) have discussed the physical implications of a measurement of primordial B -mode polarization. One can take the point of view that the inflaton ϕ is a fundamental field and assume the techniques of effective field theory, for which the heavy degrees of freedom are integrated out, to be a correct description of the physics of inflation. In this case, the effective inflaton potential can be expanded in non-renormalizable operators suppressed by some higher energy scale, for example the Planck mass:

$$V(\phi) = V_0 + \frac{1}{2}m^2\phi^2 + \phi^4 \sum_{p=0}^{\infty} \lambda_p \left(\frac{\phi}{m_{\text{Pl}}}\right)^p. \quad (6)$$

For the series expansion for the effective potential to be convergent in general and the effective theory to be self-consistent, it is required that $\phi \ll m_{\text{Pl}}$. Lyth (1997) showed that the *width* of the potential (i.e. the distance traversed by the inflaton during inflation) $\Delta\phi$, can also be related to r . The change in the inflaton field during the ~ 4 e-folds when the scales corresponding to $2 \leq \ell \leq 100$ are leaving the horizon is

$$\frac{\Delta\phi}{m_{\text{Pl}}} \sim 0.39 \left(\frac{r}{0.07}\right)^{1/2}. \quad (7)$$

According to this bound, high values of r require changes in $\Delta\phi$ to be of the order of m_{Pl} ; this is in fact only a lower bound, since at least 50-60 e-folds are required before inflation ends (e.g. Liddle & Leach (2003)), meaning that over the course of inflation, $\Delta\phi$ could exceed the bound in Eq. 7 by an order of magnitude. For the present discussion, the important point is that for a tensor-to-scalar ratio of order 0.1, the field must travel a distance $\Delta\phi \gg m_{\text{Pl}}$ over the course of inflation, so that the effective field theory description in Eq. 6 must break down at some point during inflation. This fact has been used to argue, based on self-consistency, that a very small tensor/scalar ratio is expected in a realistic inflationary universe, leading to the discouraging conclusion that the primordial B -modes in the CMB would be unobservably small.

However, arguments based on effective field theory are not the only way to study the dynamics of inflation. The inflaton may not be a fundamental scalar field; in fact, as we discuss later in § 6.2, advances are being made building “natural” particle physics-motivated inflationary models based on approximate shift symmetries and extra-dimensional setups. Also, one can take the approach that, for the predictions of single-field inflation to be valid, the only requirement is that the evolution of spacetime is governed by a single order parameter. In this approach, one can reformulate the exact dynamical equations for inflation as an infinite hierarchy of flow equations described by the generalized “Hubble Slow Roll” (HSR) parameters (Hoffman & Turner 2001; Kinney 2002; Easter & Kinney 2003; Peiris et al. 2003; Kinney et al. 2004). In the Hamilton-Jacobi formulation of inflationary dynamics, one expresses the Hubble parameter directly as a function of the field ϕ rather than a function of time, $H \equiv H(\phi)$, under the assumption that ϕ is monotonic in time. Then the equations of motion for the field and background are given by:

$$\dot{\phi} = -2M_{\text{Pl}}^2 H'(\phi), \quad (8)$$

$$[H'(\phi)]^2 - \frac{3}{2M_{\text{Pl}}^2} H^2(\phi) = -\frac{1}{2M_{\text{Pl}}^4} V(\phi). \quad (9)$$

Here, prime denotes derivatives with respect to ϕ . Equation (9), referred to as the *Hamilton-Jacobi Equation*, allows us to consider inflation in terms of $H(\phi)$ rather than $V(\phi)$. The former, being a geometric quantity, describes inflation more naturally.

This picture has the major advantage that it allows us to remove the field from the dynamical picture altogether, and study the generic behavior of slow roll inflation without making assumptions about the underlying particle physics (although the underlying assumption of a single order parameter is still present). In terms of the HSR parameters ${}^\ell\lambda_H$, the dynamics of inflation is described by the infinite hierarchy

$${}^\ell\lambda_H \equiv \left(\frac{m_{\text{Pl}}}{4\pi}\right)^\ell \frac{(H')^{\ell-1}}{H^\ell} \frac{d^{\ell+1}H}{d\phi^{\ell+1}}. \quad (10)$$

The flow equations allow us to consider the model space spanned by inflation using Monte-Carlo techniques. Since the dynamics are governed by a set of first-order differential equations, one can specify the entire cosmological evolution by choosing values for the slow-roll parameters ${}^\ell\lambda_H$, which completely specifies the inflationary model.

Note, however, two caveats: first, in practice one has to truncate the infinite hierarchy at some finite order; in this paper we retain terms up to 10th order. Secondly, the choice of slow roll parameters for the Monte-Carlo process necessitates the assumption of some priors for the ranges of values taken by the ${}^\ell\lambda_H$. In the absence of any *a priori* theoretical knowledge about these priors, one can assume flat priors with some ranges dictated by current observational limits, and the requirement that the potential satisfies the slow-roll conditions. Changing this “initial metric” of slow-roll parameters *changes* the clustering of phase points on the resulting observational plane of a given Monte-Carlo simulation. Thus, *the results from these simulations cannot be interpreted in a statistical way*.

Nevertheless, important conclusions can be drawn from the results of such simulations (e.g. Kinney (2002); Peiris et al. (2003)); they show that models do not cover the observable parameter space uniformly, but instead cluster around certain attractor regions. And these regions do not correspond especially closely to the expectations from effective field theory; they show significant concentrations of points with significant tensor/scalar ratio.

Recent work by Efstathiou & Mack (2005) shows that, in the inflationary flow picture, there is no well-defined relation of the form Eq. 7. However, a reformulation of the bound in Eq. 7 is found if one imposes observational constraints on the scalar spectral index n_s and its running with scale $dn_s/d\ln k$.

The precise values and error bars on these parameters depend on the particular data set (or combinations of data sets) used in the parameter estimation, and some data sets yield cleaner and more reliable determinations than others (Seljak et al. 2003). Nevertheless, for our purposes we shall use the tightest constraints available at present. These come from a compilation of CMB data, and large scale structure data from galaxy surveys and Lyman- α forest lines (e.g. Seljak et al. (2004)): at 95% confidence these limits are $0.92 < n_s < 1.06$ and $-0.04 < dn_s/d\ln k < 0.03$.

Here we illustrate how an empirical relation between $\Delta\phi$

and r can be found and show that this relation is somewhat insensitive to the priors on the ${}^\ell\lambda_H$ parameters.

Figures 1 and 2 show the absolute value of $\Delta\phi$ over the final 55 e-folds of inflation, plotted against the tensor-to-scalar ratio r . Fig. 1 shows a 2-million point Monte-Carlo simulation of the flow equations, allowing the fourth slow roll parameter, ${}^4\lambda_H$, to have a wide prior ${}^4\lambda_H = [-0.025, 0.025]$. This prior on ${}^4\lambda_H$ has been (arbitrarily) set to have the same width as the bound on ${}^3\lambda_H$ allowed by the WMAP data (Peiris et al. 2003). A wide prior is also allowed on the higher order HSR parameters. In the simulation shown in Fig. 2, the width of the prior on ${}^4\lambda_H$ has been decreased by a factor of five, ${}^4\lambda_H = [-0.005, 0.005]$. The higher order HSR parameters also have a narrower prior than the previous case. These choices are motivated by the prejudice that higher-order parameters in the expansion should have narrower priors around zero, and by the fact that tighter constraints on ${}^3\lambda_H$ are possible from CMB and large-scale structure data compilations or future higher-precision CMB data.

As was emphasized earlier, the top panels of these figures show that the clustering of points in the two cases is different due to the different initial distributions allowed. The bottom panels show the remaining points after the observational constraints from the above compilation of CMB and large scale structure have been applied. It is seen that with this prior in phase-space, there is now a fairly well-defined relation between $\Delta\phi$ and r , and that even though the distributions in the two simulations with initial priors of different width are different, this relationship is roughly the same in both cases. As reported in Efstathiou & Mack (2005), this reformulation of the bound in Eq. 7 is given by

$$\frac{\Delta\phi}{m_{\text{Pl}}} \simeq 6r^{1/4}. \quad (11)$$

As Efstathiou & Mack (2005) point out, the relation in Eq. 11 is so steep that, to probe models with small field variations where an effective field theory description is likely to be valid, one needs to be able to detect $r \lesssim 10^{-4}$. Conversely, a detection of a larger tensor component would support a large-field model for inflation.

Note that the discussion and the bound stated in Eq. 11 apply to non-hybrid models, plotted as dots. Figures 1 and 2 also show Monte-Carlo simulations which qualify as hybrid inflation models (e.g. Linde (1994)), plotted as stars. These indeed show a few small-field models which have significant values of r . However, it must be noted that these models inflate forever till inflation is suddenly ended at some critical time by a second field; the observables for the Monte-Carlo simulations for models in this class have been computed arbitrarily at 400 e-folds before the end of inflation for the purposes of these figures - observables computed at a different time during inflation would obviously yield different results. If a value of $r \gtrsim 10^{-4}$ is detected, hybrid models can be easily distinguished from large-field models by looking at the scalar spectral index: large-field models predict a red spectral index while hybrid models predict a blue index.

We will now try to assess the minimum level of r detectable with an idealized and a realistic CMB experiment.

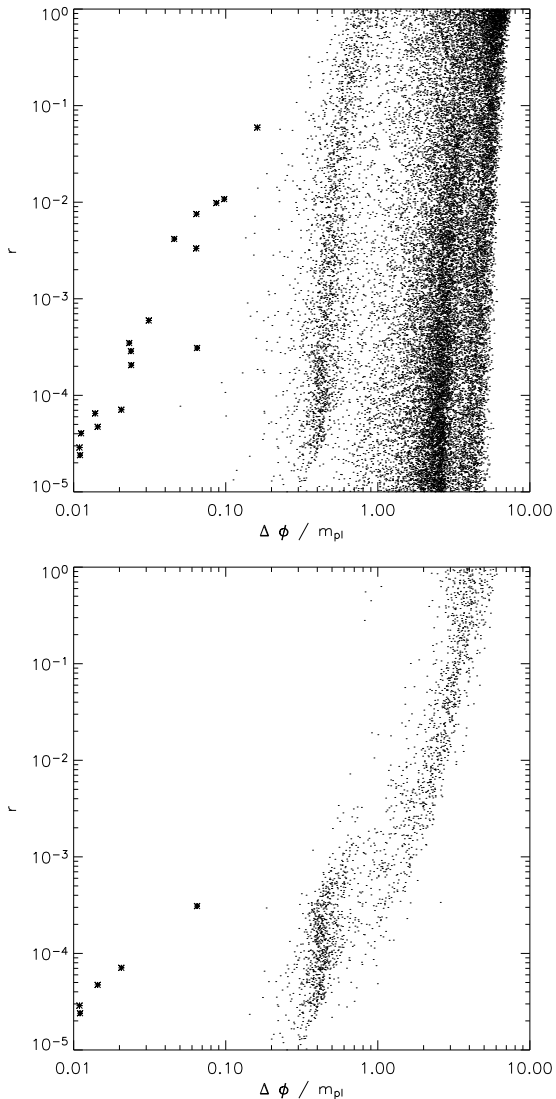


Figure 1. The absolute value of the range traversed by the scalar field ϕ over the final 55 e-folds of inflation, $\Delta\phi$, plotted against the tensor-to-scalar ratio r : (top) all models that sustain at least 55 e-folds of inflation in a 2-million point Monte-Carlo simulation to 10th order of the inflationary flow equations; (bottom) the subset of models that satisfy current observational constraints on n_s and $dn_s/d\ln k$, as discussed in the text. Hybrid models, which have $n_s > 1$, are shown as stars, and the rest as dots (see text). This simulation has a wider prior on ${}^4\lambda_H$ and higher order slow roll parameters.

3 METHOD

Here we describe the methods and the notation we will use for our error forecasts.

3.1 Definitions and Conventions

Following Bond et al. (2000), we define

$$C_\ell^{XY} = \frac{\ell(\ell+1)}{2\pi} \sum_m \frac{a_{\ell m}^X a_{\ell m}^Y}{2\ell+1}, \quad (12)$$

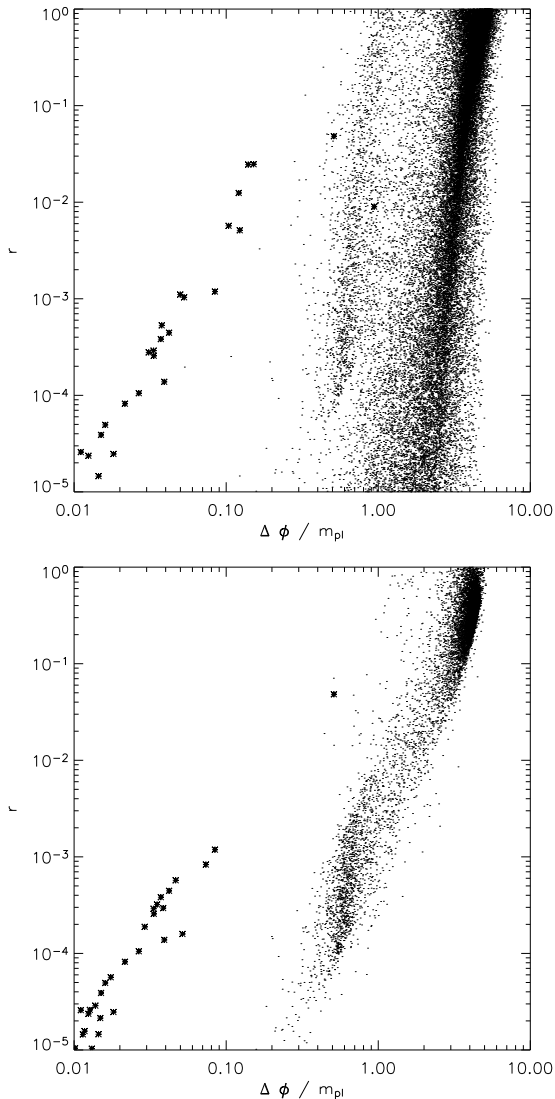


Figure 2. Otherwise identical to Fig. 1, except that the simulation shown here has a narrower prior on ${}^4\lambda_H$ and higher order slow roll parameters.

where $a_{\ell m}$ denotes the spherical harmonic coefficients, the XY superscript can be TT, TE, EE or BB , $a_{\ell m}^X$ denotes the spherical harmonic coefficients of the X signal and

$$C_\ell = \frac{\ell(\ell+1)}{2\pi} C_\ell. \quad (13)$$

For our forecast calculations, we will assume Gaussian beams: if Θ_{FWHM} denotes the FWHM of a Gaussian beam, then $\sigma_b = 0.425 \Theta_{FWHM}$.

The noise per multipole n_0 is given by $n_0 = \sigma_{pix}^2 \Omega_{pix}$ where $\Omega_{pix} = \Theta_{FWHM} \times \Theta_{FWHM} = 4\pi f_{sky} / N_{pix}$ is the pixel (beam) solid angle and N_{pix} is the number of pixels (independent beams) in the survey region and f_{sky} is the fraction of the sky covered by observations. σ_{pix}^2 is the variance per pixel, which can be obtained from the detector sensitivity s as $\sigma_{pix} = s / \sqrt{Nt}$. N is the number of detectors and t the integration time per pixel. With these conventions the noise bias becomes $\mathcal{N}_\ell = \frac{\ell(\ell+1)}{2\pi} n_0 e^{\ell^2 \sigma_b^2}$.

As the receiver temperature T_{rec} is limited to be $T_{rec} > h\nu/k$ (k is the Boltzmann constant and h is the Planck constant), the r.m.s temperature ΔT_{rms} is limited to be $\Delta T_{rms} > (T_{CMB} + T_{rec})/\sqrt{\Delta\nu\Delta t}$ where $\Delta\nu$ is the bandwidth and Δt the integration time. This limit can be overcome by using multiple detectors; for example QUIET and PolarBeaR will have of the order of 10^3 detectors.

3.2 Likelihood

Assuming that CMB multipoles are Gaussian-distributed, the likelihood function for an ideal, noiseless, full sky experiment can be written as

$$\begin{aligned}
-2 \ln \mathcal{L} &= \sum_{\ell} (2\ell + 1) \left\{ \ln \left(\frac{C_{\ell}^{BB}}{\hat{C}_{\ell}^{BB}} \right) \right. \\
&+ \ln \left(\frac{C_{\ell}^{TT} C_{\ell}^{EE} - (C_{\ell}^{TE})^2}{\hat{C}_{\ell}^{TT} \hat{C}_{\ell}^{EE} - (\hat{C}_{\ell}^{TE})^2} \right) \\
&+ \frac{\hat{C}_{\ell}^{TT} C_{\ell}^{EE} + C_{\ell}^{TT} \hat{C}_{\ell}^{EE} - 2\hat{C}_{\ell}^{TE} C_{\ell}^{TE}}{C_{\ell}^{TT} C_{\ell}^{EE} - (C_{\ell}^{TE})^2} \\
&\left. + \frac{\hat{C}_{\ell}^{BB}}{C_{\ell}^{BB}} - 3 \right\}, \quad (14)
\end{aligned}$$

where \hat{C}_{ℓ}^{XY} is the estimator for the measured angular power spectrum. The likelihood (14) has been normalized with respect to the maximum likelihood, where $C_{\ell}^{XY} = \hat{C}_{\ell}^{XY}$.

In the case of a more realistic experiment (with partial sky coverage, and noisy data) we obtain:

$$\begin{aligned}
-2 \ln \mathcal{L} &= \sum_{\ell} (2\ell + 1) \left\{ f_{sky}^{BB} \ln \left(\frac{C_{\ell}^{BB}}{\hat{C}_{\ell}^{BB}} \right) \right. \\
&+ \sqrt{f_{sky}^{TT} f_{sky}^{EE}} \ln \left(\frac{C_{\ell}^{TT} C_{\ell}^{EE} - (C_{\ell}^{TE})^2}{\hat{C}_{\ell}^{TT} \hat{C}_{\ell}^{EE} - (\hat{C}_{\ell}^{TE})^2} \right) \\
&+ \sqrt{f_{sky}^{TT} f_{sky}^{EE}} \frac{\hat{C}_{\ell}^{TT} C_{\ell}^{EE} + C_{\ell}^{TT} \hat{C}_{\ell}^{EE} - 2\hat{C}_{\ell}^{TE} C_{\ell}^{TE}}{C_{\ell}^{TT} C_{\ell}^{EE} - (C_{\ell}^{TE})^2} \\
&\left. + f_{sky}^{BB} \frac{\hat{C}_{\ell}^{BB}}{C_{\ell}^{BB}} - 2\sqrt{f_{sky}^{TT} f_{sky}^{EE}} - f_{sky}^{BB} \right\} \quad (15)
\end{aligned}$$

In Eq. 15, $C_{\ell}^{XY} = \hat{C}_{\ell}^{XY} + \mathcal{N}_{\ell}^{XY}$ where \mathcal{N}_{ℓ} denotes the noise bias, \hat{C}_{ℓ}^{XY} denotes the measured angular power spectrum which includes a noise bias contribution, f_{sky}^{XY} denotes the fraction of sky observed, $X, Y = \{T, E, B\}$ and we have allowed different fraction of the sky to be observed in T, E and B .

Note that this equation accounts for the effective number of modes allowed in a partial sky, but does not account for the mode correlation introduced by the sky cut which may smooth power spectrum features. The details of the mode-correlation depend on the specific details of the mask, but for ℓ greater than the characteristic size of the survey our approximation should hold.

The expression for the likelihood (15) is only valid for a single frequency experiment. The exact expression for multi-frequency experiments which takes into account for both auto- and cross- channels power spectra cannot be written in a straightforward manner in this form. However, for N_{chan} frequencies with the same noise level, considering both auto and cross power spectra is equivalent to having one effective frequency with an effective noise power spectrum lower

by a factor N_{chan} . This can be understood in two ways. If one were to combine N_{chan} independent maps, the resulting map will have a noise level lower by a factor $\sqrt{N_{chan}}$; thus the noise power spectrum will be that of an auto-power spectrum, reduced by a factor N_{chan} . One could instead compute auto and cross C_{ℓ} and then combine them in an minimum variance fashion. Let us assume Gaussianity for simplicity. When combining the C_{ℓ} , the covariance matrix in the absence of cosmic variance will be:

$$\Sigma_{ii'jj'} = \frac{1}{2l+1} (n^i n^j \delta_{ij} \times n^{i'} n^{j'} \delta_{i'j'} + n^i n^{j'} \delta_{ij'} \times n^{i'} n^j \delta_{i'j}) \quad (16)$$

where i, j run through the channels, $n^i n^j = N^{ij}$ and δ_{ij} denotes the Kronecker delta. Note that this has been computed for the no cosmic variance case, as there is no cosmic variance involved when combining C_{ℓ} 's computed from the same sky at different wavelengths). Thus, if N_{eff} is the same for all channels then the covariance between, say, $C_{\ell, vV}$ & $C_{\ell, vV}$ is twice that between say $C_{\ell, vW}$ & $C_{\ell, vW}$; the covariance between $C_{\ell, vV}$ & $C_{\ell, wW}$ and $C_{\ell, vW}$ & $C_{\ell, qV}$ etc. is zero. The minimum variance combination will thus yield an effective noise power spectrum of N/N_{chan} .

We can generalize the above considerations to the case where the different channels have different noise levels. This is useful for example in the case where each channel has a different residual foreground level, which, as we will show below, can be approximated as a white noise contribution in addition to the instrumental noise. The optimal channel combination would be:

$$C_l = \frac{\sum_{i,j,j \geq i} w_{i,j} C_l^{i,j}}{\sum_{i,j} w_{i,j}} \quad (17)$$

where $w_{i,j}$ are weights and are given by $[N_i N_j / 2(1 + \delta_{ij})]^{-1}$. The resulting noise will be given by

$$N_{eff} = \left(\sum_{i,j,j \geq i} \frac{1}{N_{eff,i} N_{eff,j} \frac{1}{2}(1 + \delta_{ij})} \right)^{-1/2} \quad (18)$$

3.3 Error calculation

The Fisher information matrix is defined as (Fisher 1935):

$$F_{ij} = \left\langle -\frac{\partial^2 L}{\partial \alpha_i \partial \alpha_j} \right\rangle |_{\alpha=\bar{\alpha}} \quad (19)$$

where $L \equiv \ln \mathcal{L}$ and α_i, α_j denote model parameters. The Cramer-Rao inequality says that the minimum standard deviation, if all parameters are estimated from the same data, is $\sigma_{\alpha_i} \geq (F^{-1})_{ii}^{1/2}$ and that in the limit of a large data set, this inequality becomes an equality for the maximum likelihood estimator.

For our error forecast we use the Fisher matrix approach. Thus here, α denotes a vector of cosmological parameters (we consider $\{r, n, n_t, dn/d \ln k, Z, \Omega_b h^2 \equiv w_b, \Omega_c h^2 \equiv w_c, h, \Omega_k, A(k_0)\}$, where $Z \equiv \exp(-2\tau)$), $\bar{\alpha}$ denotes the fiducial set of cosmological parameters, α_i being the i^{th} component of that vector, and \mathcal{L} is given by Eq. 15. For the fiducial parameters, we will consider three cases for $r, r = \{0.01, 0.03, 0.1\}$ and $r = 0.001, r = 0.0001$ as a special cases; for the other cosmological parameters we use $n = 1, n_t = -r/8, d \ln n / d \ln k = 0, \exp(-2\tau) = 0.72$ (corresponding to $\tau = 0.164$), $\Omega_b h^2 = 0.024, \Omega_c h^2 = 0.12, h = 0.72$,

$\Omega_k = 0$, $A(k_0) = 0.9$, in agreement with WMAP first year results (Spergel et al. 2003).

Following Spergel et al. (2003), the pivot point for n and A is at $k = 0.05 \text{ Mpc}^{-1}$ and the tensor to scalar ratio r is also defined at $k = 0.05 \text{ Mpc}^{-1}$. Making use of the consistency condition and assuming no running of the scalar or tensor spectral indices, $r(k_0)$ can be related to the r defined at any other scale k_1 by

$$r(k_1) = r(k_0) \left(\frac{k_1}{k_0} \right)^{-r(k_0)/8+1-n_s(k_0)}. \quad (20)$$

Therefore, for our choice of a scale-invariant scalar power spectrum, e.g. $r(0.05) = 0.1$ corresponds to $r(0.002) = 0.104$ and our results are thus not significantly dependent on the choice of the pivot point.

Note that for a fixed value of r , the height of the BB “reionization bump” depends on τ approximately as τ^2 , but the position of the “bump” maximum also varies. The τ determination from WMAP has a $1\text{-}\sigma$ error of ~ 0.07 (Spergel et al. 2003). Thus for a fiducial value of $\tau \sim 0.1$, one sigma below the best fit, the detectability of $r = 0.03$ ($r = 0.1$) from $\ell \lesssim 20$ is roughly⁹ equivalent to the detectability of $r = 0.01$ ($r = 0.03$) in the best fit model. On the other hand, for a fiducial value of τ one sigma above the best fit, the detectability of $r = 0.01$ ($r = 0.03$) from $\ell \lesssim 20$ is equivalent to the detectability of $r = 0.03$ ($r = 0.1$) in the best fit model. This consideration affects only large sky coverage experiments which probe the reionization bump in the BB spectrum at $\ell < 10$, and does not affect the smaller scale ground based experiments. We therefore only calculate the case of the one-sigma lower bound fiducial $\tau = 0.1$ for the space-based test case with $r = 0.001$ and the balloon-borne large angle experiment SPIDER. As a higher value for τ boosts the BB signal, we investigate this lower value of τ in order to be conservative in our predictions.

We use all the power spectrum combinations as specified in Eqs. 14 and 15, computed to $\ell = 1500$ and using the experimental characteristics specific to each experiment we study. For the partial sky experiments we add WMAP priors on n , $dn/d \ln k$, Z , $\Omega_b h^2$, $\Omega_c h^2$, h , and A .

We use the “three point rule” to compute the second derivative of L when $i = j$:

$$\frac{\partial^2 L}{\partial^2 \alpha_i} = \frac{L(\bar{\alpha} - \delta \alpha_i) - 2L(\bar{\alpha}) + L(\bar{\alpha} + \delta \alpha_i)}{\delta \alpha_i^2}. \quad (21)$$

Here, by $L(\bar{\alpha})$ we mean L evaluated for the fiducial set of cosmological parameters. $\bar{\alpha} + \delta \alpha_i$ denotes the vector of cosmological parameters made by the fiducial values for all elements except the i^{th} element, which is $\bar{\alpha}_i + \delta \alpha_i$; $\delta \alpha_i$ is a small change in α_i .

For $i \neq j$ we use:

$$\frac{\partial^2 L}{\partial \alpha_i \partial \alpha_j} = \frac{\{ [L(\bar{\alpha} + \delta \alpha_i + \delta \alpha_j) - L(\bar{\alpha} + \delta \alpha_i - \delta \alpha_j)] [L(\bar{\alpha} - \delta \alpha_i + \delta \alpha_j) - L(\bar{\alpha} - \delta \alpha_i - \delta \alpha_j)] \}}{2 \delta \alpha_i 2 \delta \alpha_j} \quad (22)$$

where $\bar{\alpha} + \delta \alpha_i - \delta \alpha_j$ denotes a vector of cosmological parameters where all components are equal to the fiducial cos-

mological parameters, except components i and j which are $\bar{\alpha}_i + \delta \alpha_i$ and $\bar{\alpha}_j - \delta \alpha_j$ respectively.

For high multipoles the Central Limit Theorem ensures that the likelihood is well approximated by a Gaussian. Thus, if one also neglects the coupling between TT , TE and EE , the high ℓ Fisher matrix can be well approximated by

$$-2 \left\langle \frac{\partial \ln \mathcal{L}}{\partial \alpha_i \partial \alpha_j} \right\rangle |_{\alpha=\bar{\alpha}} = \sum_{P,\ell} \frac{\partial C_\ell^P}{\partial \alpha_i} \Sigma_{\ell\ell'}^{-1} \frac{\partial C_{\ell'}^P}{\partial \alpha_j}, \quad (23)$$

where $P = TT, EE, BB, TE$, and Σ denotes the covariance matrix. Therefore the Fisher matrix calculation can be sped up greatly by precomputing $\frac{\partial C_\ell^P}{\partial \alpha_i}$. However, since most of the r signal comes from low ℓ , we will not use this approximation here.

3.4 Detection vs Measurement

There are two different approaches in reporting an experiment’s capability to constrain r . In the first approach, one considers the null hypothesis of zero signal (i.e. $r = 0$); then one asks with what significance a non-zero value of r could be distinguished from the null hypothesis. This approach gives the statistical significance of a detection, but it does not yield a measurement of r . To obtain a measurement of r with an error-bar, a different approach is needed. In this case, the value of r is obtained via a Bayesian maximum likelihood analysis, and the cosmic variance contribution for non-zero r is included in the error calculation. Since a measurement of r is needed to constrain inflationary models, here we follow the second approach. Thus we do not report the minimum value of r that can be distinguished from zero, but error-bars for several fiducial r values.

4 FOREGROUNDS

As anticipated in the introduction, foregrounds are one of the main obstacles to the detection and measurement of primordial B -modes: they are likely to dominate the signal at all frequencies. And, while foreground intensities are relatively well known, polarized foregrounds are not. Here we will neglect the effect of foregrounds on the CMB temperature, as foreground contamination in the temperature data at the angular scales considered is much smaller than the contamination to the polarized signal and foreground cleaning is expected to leave a negligible contribution in the temperature signal (Bennett et al. 2003b).

CMB polarized foregrounds arise due to free-free, synchrotron, and dust emission, as well as due to extra-galactic sources such as radio sources and dusty galaxies. Here, we will consider only synchrotron and dust emission; in fact, free-free emission is expected to be negligibly polarized, and the radio source contribution remaining after masking the sky for all sources brighter than ~ 1 Jy is always well below other foregrounds at large angular scales. E.g. Tucci et al. (2004) find that this residual point source contribution is $\lesssim 1\%$ of the other foregrounds in the power for $\ell \lesssim 200$. Note, however, that at $\ell \gtrsim 100$, this contribution that we neglect can be as important in the BB power spectrum as

⁹ Note that since the “bump” location changes as τ changes this argument is only qualitative.

the lensing signal (see Tucci et al. (2004)), and therefore can seriously hinder the delensing implementation.

We also neglect the contribution from dusty galaxies.

4.1 Synchrotron

Free electrons spiral around the Galactic magnetic field lines and emit synchrotron radiation. This emission can be up to 75% polarized, and is the main CMB foreground at low frequencies. We model the power spectrum of synchrotron as (e.g. Tegmark et al. (2000); de Oliveira-Costa et al. (2003)):

$$C_{\ell}^{S,XY} = A^S \left(\frac{\nu}{\nu_0} \right)^{2\alpha_S} \left(\frac{\ell}{\ell_0} \right)^{\beta_S} \quad (24)$$

where we have assumed that Galactic synchrotron emission has the same amplitude for E and B . The unpolarized synchrotron intensity has $\alpha_S \sim -3$ with variations across the sky of about $\Delta\alpha_S \sim 0.15$ (e.g. Platania et al. (1998, 2003); Bennett et al. (2003b)) and $\beta_S \simeq -3$ (e.g. Giardino et al. (2002) and references therein) with variation across the sky¹⁰. Information on polarized synchrotron is limited at present to frequencies much lower than CMB frequencies (e.g. Carretti et al. (2005a); Carretti et al. (2005a) and mostly low Galactic latitudes).

Recent estimates for β_S for polarized synchrotron emission (Tucci et al. 2002; Bruscoli et al. 2002) show spatial and frequency variations. For example, Bruscoli et al. (2002) study the angular power spectrum of polarized Galactic synchrotron at several frequencies below 3 GHz and at several Galactic latitudes, and find a wide variation mostly due to Faraday rotation and variations in the local properties of the foregrounds. Bernardi et al. (2004) find that at high galactic latitudes there is no significant dependence of the slope on frequency. Here we consider $\beta_S = -1.8$ for both E and B , consistent with e.g. Baccigalupi et al. (2001); Bruscoli et al. (2002); Bernardi et al. (2004, 2003).

We take the reference frequency of $\nu_0 = 30$ GHz and the reference multipole $\ell_0 = 300$ so that we can use the DASI 95% upper limit (Leitch et al. 2005) of $0.91 \mu\text{K}^2$ to set the amplitude A_S . Since the normalization is set at $\ell = 300$ and most of the r signal is at $\ell < 100$, a choice of a flatter β_S would have the effect of reducing the synchrotron contamination at low ℓ .

We will consider three cases: an amplitude equal to the DASI limit (pessimistic case) and half of that amplitude (reasonable case). Recent results by Carretti et al. (2005a) show a detection of synchrotron polarized emission in a clean area of the sky at 2.3 GHz. The amplitude of this signal is about an order of magnitude below the DASI upper limit. We will consider this amplitude (10% of the DASI limit) as a minimum amplitude (optimistic case) achievable only for partial sky experiments which can look at a clean patch of the sky. Unless otherwise stated we will assume the pessimistic case.

4.2 Dust

We ignore a possible anomalous dust contribution (e.g. Finkbeiner et al. (2004); Draine & Lazarian (1998)) as it is important only at frequencies below 35 GHz or so (Lazarian & Finkbeiner 2003). We model the dust signal as:

$$C_{\ell}^{D,XY} = p^2 A^D \left(\frac{\nu}{\nu_0} \right)^{2\alpha_D} \left(\frac{\ell}{\ell_0} \right)^{\beta_D^{XY}} \left[\frac{e^{h\nu_0/KT} - 1}{e^{h\nu/KT} - 1} \right]^2 \quad (25)$$

assuming the temperature of the dust grains to be constant across the sky, $T = 18\text{K}$. We take $\alpha_D = 2.2$ (Bennett et al. 2003b), and set our reference frequency to be $\nu_0 = 94$ GHz. The amplitude A^D is given by the intensity normalization of Finkbeiner et al. (1999), extrapolated to 94 GHz, and p is the polarization fraction. Since we want to use the Archeops upper limit for the diffuse dust component (Benoît et al. 2004) of $p = 5\%$ at $\ell = 900$ (roughly corresponding to the resolution in Benoît et al. (2004)), we set $\ell_0 = 900$. Archeops finds $\alpha_D = 1.7$; with our choice the extrapolation of the dust contribution at higher frequency is slightly more conservative. Since a weak Galactic magnetic field of $3 \mu\text{G}$ already gives a 1% (Padoan et al. 2001) polarization, the polarization fraction should be bound to be between 1–5%. Unless otherwise stated, we will assume a 5% polarization fraction. For $C_{\ell}^{XY,D}$ we follow Lazarian & Prunet (2002); Prunet et al. (1998): $\beta_D^{EE} = -1.3$, $\beta_D^{BB} = -1.4$, $\beta_D^{TE} = -1.95$, $\beta_D^{TT} = -2.6$ (in agreement with the measurement of starlight polarization of Fosalba et al. (2002)).

As parameters like β_D^{XY} , β_S^{XY} , α_D , α_S and p may show spatial variations, the optimal frequency band may be different for full sky and partial sky experiments and may vary between different patches of the sky.

4.3 Propagation of foreground subtraction errors

The foreground treatment presented above is quite simplistic and cannot capture the foreground properties completely. However, we will not be using these estimates to subtract the foreground from the signal. Instead, we assume that foreground subtraction can be done correctly down to a given level (e.g. 1%, 10%), and use these foreground models to propagate the effects of foreground subtraction residuals into the resulting error-bars for the cosmological parameters. In other words the modeling enters in the error-bars, not in the signal. Therefore, as long as the foreground assumptions are reasonable, and foregrounds can be subtracted at the assumed level, the results are relatively insensitive to the details of the foreground model. Of course, one cannot know in advance whether the foreground will be subtracted at that level. For this reason we considered several different options (10%, 1% etc.).

To propagate foreground subtraction errors we proceed as follows. We assume that foregrounds are subtracted from the maps via foreground templates or using multi-frequency information with techniques such as MEMs (e.g. Bennett et al. (2003b)), ICA (Baccigalupi et al. 2004; Stivoli et al. 2005). We write the effect on the power spectrum of the residual Galactic contamination as an additional “noise-like” component $C_{\ell}^{res,fg,XY}$ composed by a term proportional to the foreground C_{ℓ} and a noise term:

$$C_{\ell}^{res,fg,XY}(\nu) = C_{\ell}^{fg,XY}(\nu)\sigma^{fg,XY}$$

¹⁰ At low Galactic latitudes, the synchrotron index shows a flattening, but we assume here that the mask will exclude those regions

$$+ N^{fg,XY} \left(\frac{\nu}{\nu_{tpl}} \right)^{-2\langle\alpha_{fg}\rangle} \quad (26)$$

where fg denotes dust (D) or synchrotron (S), $\langle\alpha_{fg}\rangle$ denotes the average value of the spectral index, and $\sigma^{fg,XY}$ quantifies how good the foreground subtraction is (e.g. $\sigma^{fg,XY}=0.01$ for a 1% residual in the C_ℓ). $C_\ell^{fg,XY}$ is given by Eq. 24 for synchrotron and Eq. 25 for dust; $N^{fg,XY}$ denotes the noise power spectrum of the template map. As an estimate, we assume that the noise spectrum in the template maps is a white noise equal to the noise spectrum of one of the channels reduced by a factor $1/2 \times n(n-1)/2$. The factor of $1/2$ arises from the fact that foreground templates are effectively obtained by subtracting maps at two different frequencies (which increases the noise in the map by a factor $\sim\sqrt{2}$), and that there are $n(n-1)/2$ map pairs. Although the map pairs are not all independent, we expect that experiments will have some channels both at higher and lower frequencies than those devoted to cosmology, to be used for foreground studies. We thus consider this a reasonable estimate for the template noise.

ν_{tpl} denotes the frequency at which the template is created. For this forecast we assume that ν_{tpl} coincides with the frequency of the experiment channel where the foreground contamination is highest. To justify the *ansatz* Eq. (26), consider the result from Tucci et al. (2004) (their §3 and Appendix).

$$C_\ell^{res,fg,XY} = \frac{(\ln(\nu_0/\nu))^2}{16\pi} \times \sum_{\ell_1} (2\ell_1 + 1) C_{\ell_1}^{fg,XY} \sum_{\ell_2} (2\ell_2 + 1) C_{\ell_2}^{\alpha_{fg}} \begin{pmatrix} \ell & \ell_1 & \ell_2 \\ 2-2 & 0 & 0 \end{pmatrix}^2 + C_\ell^{XY,\Delta fg} \left(\frac{\nu}{\nu_0} \right)^{-2\langle\alpha_{fg}\rangle} \quad (27)$$

where $C_\ell^{\alpha_{fg}}$ denotes the power spectrum of the spectral index error. If the power spectrum of the spectral index error has the same ℓ dependence as the total intensity power (that is $\sim\ell^{-3}$ for synchrotron and $\sim\ell^{-2.6}$ for dust), neglecting the logarithmic dependence on ν we obtain Eq. 26. We assume that the foreground template is computed for the ‘‘cosmological’’ frequency where the foreground contamination is highest. For example, for 5 different frequency bands at (30, 50, 90, 100, 200 GHz), the synchrotron template will be computed for the 30 GHz band and the dust template for the 200 GHz band.

4.4 Delensing

Several different techniques to reconstruct the gravitational lensing potential from CMB data and reduce or remove lensing contamination to the BB signal have been proposed (Hu & Okamoto 2002; Kesden et al. 2002; Knox & Song 2002; Okamoto & Hu 2003; Kesden et al. 2003). However, in presence of instrumental noise the contamination cannot be easily removed. In addition foreground emission is expected to be highly non-Gaussian and the performance of delensing techniques have not been explored in the presence of non-Gaussian foregrounds. In fact, the separation of the primordial gravitational wave contribution is achieved exploiting the non-Gaussianity of the lensed CMB. Thus, the non-Gaussian nature of the foregrounds will degrade this re-

construction and limit the delensing performance. To include the above considerations, forecast whether delensing can successfully be implemented and can improve constraints on r we proceed as follows. If foregrounds are neglected, we assume that the delensing technique can be applied only in the signal-dominated regime, and that in this regime the procedure can reduce the BB -lensing signal only down to the level of the instrumental noise power spectrum. This assumption is well motivated by results of e.g., Seljak & Hirata (2004). When including foregrounds, we assume that delensing can be implemented only if the BB power spectrum of the combination of foreground emission and foreground template noise is below 10% of the BB lensing power spectrum, and that the BB -lensing signal can be reduced only down to 10% of the foreground signal (emission plus template noise). We deem this to be a reasonable assumption: a percent level of foreground contamination in the angular power spectrum is probably close to the minimum achievable and it corresponds to a 10% level in the maps. The residual foreground will be highly non-Gaussian thus limiting the delensing to this level. When considering a realistic case with noise and foregrounds, for every ℓ we consider whichever effect is most important.

5 CASES WE CONSIDER

We consider several different experimental settings. First an ideal experiment (IDEAL), then a more realistic full-sky satellite experiment (SATEL) and finally, ground-based and balloon-born partial sky experiments. For all these cases, we compute the marginalized errors on the parameters using the Fisher matrix approach illustrated above. In the main text of the paper we report errors for the parameters relevant for inflation and parameters degenerate with these (i.e. r , n , n_t , $dn/d\ln k$ and Z). The errors on the other cosmological parameters are reported in the Appendix. For each case we start by considering ten cosmological parameters (r , n , n_t , $dn/d\ln k$, Z , w_b , w_c , h , Ω_k and A). We do not consider calibration uncertainties, even though they propagate into the error on the amplitude. As exploring non-flat models is computationally expensive when we find that Ω_K is only degenerate with h , we impose flatness (FLT). This constraint does not affect the estimated error on the remaining cosmological parameters. Finally, we report errors obtained with and without imposing the consistency relation ($n_t = -r/8$, CR).

5.1 Ideal experiment

Let us consider an ideal experiment, covering the full sky, with no instrumental noise and no foregrounds. We consider $\ell_{max}=1500$ because smaller angular scales will be observed from the ground and, most importantly, because higher multipoles in the temperature are affected by secondary effects while in the polarization $\ell > 1500$ does not add significant cosmological information.

Since Hirata & Seljak (2003); Seljak & Hirata (2004) showed that the lensing contribution to the BB spectra can be greatly reduced and, in the absence of instrumental noise and foregrounds, completely eliminated, we consider two cases: the BB spectrum with lensing (L) and without

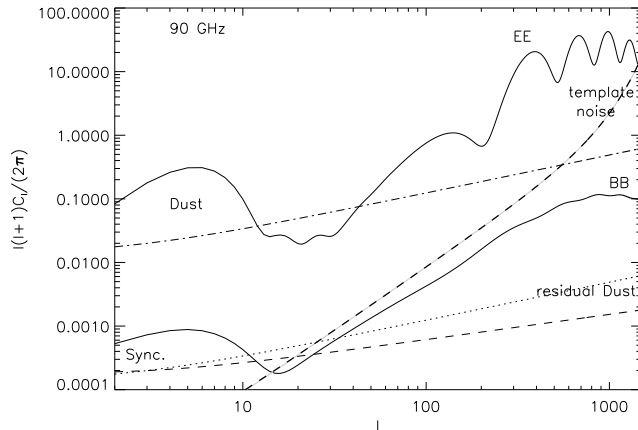


Figure 3. *EE* and *BB* signal for $r = 0.03$ fiducial model, maximum estimated foreground level and foreground residuals for 1% foreground subtraction at 90 GHz. Synchrotron is normalized to the DASI upper limit at $\ell = 300$ 30GHz assuming a frequency dependence of ν^{-3} . Dust is normalized so that at 94 GHz, $\ell = 900$ dust is 5% polarized. The template noise is that expected for the hypothetical satellite experiment.

Table 1. $1-\sigma$ errors for an ideal experiment, including lensing (L), with no lensing (NL).

	r	Δr	Δn	Δn_t	$\Delta dn/d \ln k$	ΔZ
L	0.01	0.001	0.0017	0.056	0.003	0.003
	0.03	0.0027	0.0017	0.047	0.0036	0.003
	0.1	0.006	0.002	0.035	0.0035	0.0035
NL	0.01	0.000021	0.0021	0.0019	0.0038	0.0038
	0.03	0.000063	0.0021	0.0019	0.0038	0.0038

Table 2. Ideal experiment, $\ell_{max} = 1500$, n_t fixed by consistency relation (CR)

r	Δr L	Δr NL
0.01	4.5×10^{-4}	1.6×10^{-5}
0.03	7.4×10^{-4}	4.9×10^{-5}

(NL) (i.e. with the lensing contribution perfectly subtracted out).

We report the results in table Table 1 In the L case, due to the lensing contamination, the same error can be achieved by considering only $\ell \leq 300$ for *BB*. Errors on other relevant cosmological parameters are reported in Table 1. We find that r is mainly degenerate with n_t ; by fixing n_t , the error on r is greatly reduced (see Table 2), but the errors on the other cosmological parameters do not change significantly.

If lensing can be completely subtracted from the *BB* spectrum, we obtain that the error bars on r improve by more than an order of magnitude (see Table 6).

5.2 Space-based experiment

We next consider a full-sky (space-based) experiment with a beam of FWHM 8 arcminutes, 5 frequency channels ($N_{chan} = 5$) at 30, 50, 70, 100, 200 GHz, and a sky cov-

Table 3. Realistic satellite experiment, no foreground, no lensing subtraction, marginalized errors, $\ell_{max} = 1500$. The error on the running is $\Delta dn/d \ln k = 0.0046$ in all these cases.

case	r	Δr	Δn	Δn_t
NO FG	0.01	0.003	0.0023	0.098
	0.03	0.0048	0.0023	0.069
	0.1	0.01	0.0023	0.056
NO FG CR	0.01	0.0011	0.0023	–
	0.03	0.0017	0.0023	–
	0.1	0.0028	0.0023	–

erage of 80%. Since the Galactic emission is highly polarized we consider that a realistic Galactic cut will exclude about 20% of the sky. We start by assuming a noise level of $2.2 \mu K$ per beam per frequency channel. This noise level is achievable with the next generation space-based experiments, and is well-matched to measure the first peak in a possible $r = 0.01$ gravity wave signal in the cosmic variance-dominated regime. We will then explore the effect of a higher (lower) noise level on the errors on r . As before, our maximum multipole will be $\ell_{max} = 1500$. Finally we will explore how the constraints can be improved by implementing delensing.

We first consider an idealized case where there are no foregrounds. The constraints on r , n , and n_t are reported in table 3, the error on $dn/d \ln k$ is $\Delta dn/d \ln k = 0.0046$ in all these cases. When imposing flatness these constraints are virtually unchanged. Marginalized constraints on the other parameters are reported in the Table 6.

Thus, we see that in the absence of foreground contamination, a realistic experiment with this noise level can achieve constraints close to those for an ideal experiment for our fiducial values of r . We find that the noise level can be higher by a factor 10 before the constraints get significantly degraded. In particular we find that for $r = 0.03$ a noise level

of $22 \mu\text{K}$ per beam increases the error on r by an order of magnitude with respect to the zero-noise case.

Since the noise is not the limiting factor for the values of r considered here, we conclude that reducing the sky coverage of such an experiment to reduce the noise level would not improve the signal to noise.

5.2.1 Delensing

To take into account of the possibility of improving the signal-to-noise by applying the “delensing” (DL) technique we proceed as follows. We start by ignoring foregrounds and consider only the effect of instrumental noise. Since in the noise-dominated regime (i.e. when the power spectrum of the noise is greater than the BB -lensing power spectrum), we assume that delensing cannot be successfully implemented, we find¹¹ that for our realistic satellite experiment, delensing does not significantly improve the constraints on the relevant parameters. In other words, for the noise level considered, the signal-dominated regime for lensing is too small to help improve constraints significantly.

Thus, in the absence of foregrounds, reducing the sky coverage to lower the noise would help such a space-based experiment to access the primordial signal at the “peak”. However, partial sky experiments can be done much more cheaply from the ground or from a balloon and can reach even lower noise levels. We shall see below how these conclusions can change in the presence of foregrounds.

5.2.2 Foregrounds

We find that even in the pessimistic case for the foreground amplitude (for both dust and synchrotron), if foregrounds can be subtracted at the 1% level ($\sigma^{fg,XY} = 0.01$) and channels can be optimally combined to minimize the effect of the residual contamination, the additional noise-like component C_ℓ^{res} is comparable to or smaller than the instrumental noise of $2.2 \mu\text{K}$ per beam. In particular, we find that the total effective noise (that is, instrumental noise plus foreground subtraction residuals) is higher than the instrumental noise contribution by a factor ~ 3 at $\ell = 2$, but only a factor of ~ 1.4 at $\ell = 10$ and ~ 1.1 at $\ell > 100$. As a result, the constraints on cosmological parameters are not significantly affected by the presence of a residual foreground contamination at this level. Note that we do not propagate into the error bars a possible uncertainty on the residual foreground contamination, as this will be a higher-order effect in our approach; in other words we assume that the uncertainty in the residual foreground contamination is negligible compared with the residual contamination level. When dealing with realistic data the validity of this assumption will need to be assessed.

In order for the foregrounds to be subtracted at the percent level, a drastically improved knowledge of the amplitude and the spectral and spatial dependence of polarized

foreground emission is needed. This can be achieved by observing the polarized foreground emission on large areas of the sky, at high galactic latitudes, with high resolution and high sensitivity and at multiple wavelengths, both at higher and lower frequencies than the “CMB window”. Most likely, a combination of approaches will be needed. For example, the Planck satellite will observe the full sky polarization up to 350 GHz and down to 30 GHz. The proposed BLAST-Pol (M. Devlin, private communication) will survey smaller regions of the sky at higher sensitivity and at higher frequencies, enabling one to extrapolate the dust emission more securely. The ability to create accurate foreground templates and to reduce foreground contamination will depend crucially on the success of these efforts.

As a foreground residual of 1% may be too optimistic, we also consider cases with a 10% foreground residual in the power spectrum. We find that, while for level of foreground residuals of 10 constraints on the recovered parameters degrade rapidly.

Our fiducial values for r (0.01, 0.03 and 0.1) have been chosen because they are accessible to experiments in the very near future. A detection of such a large primordial tensor component would support a large-field model (see also the discussion of hybrid inflation models in §2). Following the considerations of Efstathiou & Mack (2005), it would imply that, if the inflaton is a fundamental field, the effective field theory description is not valid, i.e. that Eq. 6 is not a self-consistent description of inflation.

Thus, we also investigate lower values of r of 10^{-3} and 10^{-4} which are closer to satisfying the effective field theory description (see Table 4). We find that a three- σ detection of $r = 10^{-3}$ is realistically achievable if the foreground contamination is lower than the DASI upper limit and if foreground cleaning can reduce contamination at least to the 1% level in the power spectrum. However a value of $r = 10^{-4}$ cannot be detected by this realistic experiment given our noise level and estimates of foregrounds. To assess whether the limiting factor for detecting such a gravity wave signal is the noise level or foreground contamination, we computed the expected errors for a case with no noise, synchrotron amplitude 1/2 of the DASI limit, dust polarization fraction of 5% and foreground subtraction at the 1% level. Imposing the consistency relation we find that $\Delta r = 6 \times 10^{-5}$, not even a two- σ detection. This implies that the main obstacle to detecting such a small value of r will come from Galactic foregrounds. To assess quantitatively how much the r detection could be degraded by a lower value of τ we also report the errors for a fiducial model with $r = 0.01$ and $\tau = 0.1$.

As the delensing implementation in this case is limited by foregrounds residuals, not by the noise level, it would not help for a space-based experiment to reduce the sky coverage by a factor of a few, say, to reduce the noise levels. As we will see below, delensing could be implemented by targeting a small region of the sky with particularly clean foregrounds. However, this can be done more easily and cheaply from the ground.

Finally we note that, although we used the full combination of T , E and B data, the signal for r comes from the BB signal. In fact, we find that if we consider our realistic satellite case but only T and E -mode polarization data, only upper limits can be imposed on r for $r < 0.1$.

¹¹ For greater computational speed we have fixed Ω_k to be zero for this calculation. We find that this affects only the error on the Hubble parameter which is not the main focus of the present work.

Table 4. Realistic satellite experiment including foregrounds for $r \leq 10^{-3}$ and flat cosmology. We have assumed that synchrotron emission amplitude is 50% of DASI limit, a dust polarization fraction 5% and that foregrounds can be subtracted to 1% in the power spectrum. For comparison we also report a case for no instrumental noise. In the latter case, the error on r is reduced only by a factor ~ 2 , indicating that foregrounds contamination becomes the limiting factor.

case	r	Δr	Δn	Δn_t	$\Delta dn/d \ln k$
SAT	0.0001	0.00019	0.0023	0.43	0.0046
	0.001	0.0013	0.0023	0.31	0.0046
+CR	0.0001	0.00012	0.0023	–	0.0046
	0.001	0.0003	0.0023	–	0.0046
SAT $\tau = 0.1$	0.001	0.0020	0.002	0.47	0.0045
	+CR	0.001	0.00043	0.002	–
NO NOISE	0.0001	0.00007	0.0019	0.17	0.0037
	+CR	0.0001	0.000057	0.0019	–

5.3 Ground-based and balloon-borne experiments

While a space-based experiment may be a decade away, in the shorter term, partial-sky ground-based experiments will be operational in the next few years. Ground-based experiments are less expensive and can achieve a lower level of noise contamination at the expense of covering a smaller region of the sky. However, as the primordial signal is minimal at $10 < \ell < 30$, the signal-to-noise is expected to scale only as the square root of the sky fraction for experiments covering more than about 200 square degrees (for the same noise level, frequency coverage and angular resolution).

For $r = 0.03$, the primordial B -mode signal dominates the lensing one on scales of 5-10 degrees ($\ell \lesssim 70$), but for $r = 0.01$, it dominates only on scales larger than $\text{few} \times 10$ degrees ($\ell \lesssim 10$). So ground-based experiments may need to target a clean patch of the sky and will need to rely on delensing to detect r values $\lesssim 0.03$.

On the other hand, the amplitude of the large-scale B -mode signal strongly depends on the value for τ ; thus a limit on r from these scales is somewhat more cosmology-dependent.

Here we consider several ground-based and balloon-borne experiments; the full set of experimental specifications assumed for each of these are reported in the Appendix (Table 7).

Continuously changing the sky coverage, frequency coverage and number of frequencies, number of detectors and angular resolution for these experiments will be prohibitive. But we want to concentrate on experimental setups that can be made with next generation technology; hence we report here results for a few selected experimental designs that we found already make the best use of next generation technology. We will then consider small variations around these setups. We will also discuss in the text results for selected combinations of r and foreground assumptions and report all other cases considered in Table 6.

Firstly, we consider two instruments with the specifications of the ground-based experiments QUIET and PolarBeaR (based on HEMPT and bolometer technology respectively), and two possible combinations of these experiments, ensuring wider frequency coverage. Of these,

QUIET+PolarBeaR is a straight combination of the frequency channels and noise properties of QUIET and PolarBeaR. QUIETBeaR is a hypothetical experiment with the detectors of QUIET with added channels at the PolarBeaR frequencies, but with the QUIET 90 GHz noise properties, designed to observe a significantly smaller area of the sky. The motivation behind this combination is to check the improvement in constraints in an experiment where it is possible to successfully implement delensing. Finally, we consider a balloon-based experiment with the properties of SPIDER (J. Ruhl private comm.).

The ground-based experiments considered above obtain their r constraint principally by going after the primordial BB “first peak” in the ℓ -range 70-100. On the other hand, the larger sky coverage of the balloon-borne experiment makes it possible for it to access the “reionization bump” at large scales, where the primordial signal may dominate significantly over the weak lensing, depending on the value of τ . Therefore, this selection of experiments pretty much cover the possibilities of what can be done without going to space.

We find that QUIET can detect $r = 0.1$ at the $3\text{-}\sigma$ level when imposing the consistency relation, if foregrounds can be subtracted at the 1% level (see Table 5). Alternatively if foregrounds can only be cleaned at the 10%, the experiment should observe a clean patch of the sky (with minimal foreground emission) needs to be observed to achieve the same signal-to-noise.

Since we assume that delensing can be implemented only where the B -lensing power spectrum is 10 times higher than the foreground emission and template noise, we find that delensing cannot be implemented for our pessimistic foreground levels. It could be implemented for a clean patch of the sky where the synchrotron amplitude is 1/10 of the DASI limit and dust polarization fraction is $\sim 1\%$. In this case, the limiting factor for delensing becomes the noise in the foreground templates. We find that the error-bars are not significantly changed and $r = 0.01$ is still out of reach (Table 6).

An experiment like PolarBeaR can improve on these constraints on r if the dust contamination is minimal (1% of dust contamination according to our assumptions; Table 5).

However, an aggressive level of foreground cleaning, as the one considered here, can realistically be achieved only with a wider frequency coverage well below and above the cosmological window. Moreover, additional frequencies enable one to reduce the foreground template noise and make delensing possible. The QUIETBeaR and QUIET+PolarBeaR channel combination, with the addition of higher frequencies, improves dust cleaning; lower frequencies will be useful for improving synchrotron subtraction. We find that the QUIET+PolarBeaR combination in a clean patch of sky (50% of DASI limit and 1% dust polarization) with good foreground subtraction can detect $r = 0.1$ at better than the $3\text{-}\sigma$ level and $r = 0.03$ at about $3\text{-}\sigma$ level.

On the other hand, delensing can be implemented if a small, clean patch of the sky is observed with high sensitivity. In our analysis, if an experiment like QUIETBeaR can achieve 1% foreground cleaning and can observe a particularly clean patch of the sky, we forecast that delensing can be successfully implemented; thus $r = 0.01$ can be de-

Table 5. Ground-based and balloon-borne experiments (see Table 7 for specifications), including instrumental noise and foregrounds, for flat cosmologies. $\tau = 0.164$ has been taken to be the fiducial value unless explicitly stated otherwise. We have used WMAP priors on cosmological parameters as explained in the text.

case	r	Δr	Δn
QUIET	0.01	0.015	0.029
FG 1%	0.03	0.019	0.03
CR	0.1	0.035	0.03
QUIETBeaR DASI10%,dust1% FG1% CR DL	0.01	0.003	0.054
PolarBeaR	0.01	0.012	0.018
DASI50%,dust1%	0.03	0.015	0.018
FG1% CR	0.1	0.023	0.018
QUIET+PolarBeaR	0.01	0.006	0.015
DASI50%,Pol1%	0.03	0.009	0.02
FG1% CR	0.1	0.017	0.02
SPIDER, $\tau = 0.1$ DASI50%,Pol1% FG1% CR	0.01	0.004	0.1

tected at the $\sim 3\text{-}\sigma$ level if imposing the consistency relation (Table 5).

Note, however, that at small angular scales, extragalactic point source contamination – which we have neglected – may have an amplitude comparable to that of the lensing signal, making delensing implementation even harder.

The specifications of the SPIDER experiment are not too dissimilar from those of the realistic satellite experiment considered above. The slightly different frequency coverage and noise level, the different beam size and the fact that the remaining fraction of the sky after the Galactic cut is 40%, change the forecast errors only slightly. For example for a fiducial model with $\tau = 0.1$, $r = 0.01$ can be detected at the $2\text{-}\sigma$ level in the presence of noise and foregrounds. Thus, the same considerations for the satellite experiments apply here. We report forecasts for SPIDER in Tables 5 and 6. Note that the errors on other parameters which are mostly constrained by the temperature data at $\ell > 300$ such as n , w_b etc. are larger than for our satellite experiment. This is because the beam size of SPIDER is not optimized for this. The error on r for the CR case is only a factor of a few larger than for a satellite experiment for $\tau = 0.1$. Such an experiment could perform two flights, one in the northern hemisphere and one in the southern hemisphere, and thus cover a larger fraction of the sky. Assuming that the two maps can be accurately cross-calibrated we find that the errors on r could be reduced scaling approximately like $\sqrt{f_{sky}}$.

6 CONCLUSIONS

One issue that we have not discussed is that, while on the full sky E and B modes are separable, this is no longer the case when only small patches of the sky are analyzed, as the boundaries of the patch generate mode mixing. The smaller the patch, the more important the effect

of the boundary is expected to be. In the absence of foregrounds, Lewis, Challinor & Turok (2002) showed that for simple patch geometries, E and B modes can still be separated. In particular, for circular patches larger than about 5 degrees in radius, they find that the degradation due to imperfect $E\text{-}B$ separation is negligible. However, for more general patch shapes this may be optimistic. All the experiments we considered had patches comfortably larger than this limit, and therefore we expect that this effects should not degrade our forecasts significantly.

From the above results we can deduce some general considerations which may help in planning, designing and optimizing future B -mode polarization experiments. Given the realistically achievable constraints on r , we can then forecast what can be learned about inflationary physics from these experiments. In our forecast, we have also neglected “real world” effects that are experiment-specific such as inhomogeneous/correlated noise, $1/f$ effects, etc. But these effects are not expected to significantly alter our conclusions (POLARBeaR and QUIET collaborations, private comm.).

6.1 Guidance for B -mode polarization experiments

Our assumptions about foregrounds contamination are based on information coming from much lower or higher frequencies than the CMB window, and in many cases from observations of patches of the sky. Since the properties of the polarized foregrounds show large spatial variations across the sky, the optimal “cosmological window” may depend strongly on the area of the sky observed and may be different for full sky or partial sky experiments. In addition, experiments working below ~ 70 GHz will want to concentrate in sky regions with low synchrotron contamination, while experiments at higher frequencies need to focus regions with low dust: one “recipe” may not “fit all”. Due to our limited polarized foreground knowledge it is not yet possible to make reliable predictions on which areas of the sky will be the cleanest and more suitable for primordial B -mode detection (or if the experiments considered here, by reducing their sky coverage, could be less contaminated by foregrounds). However forthcoming datasets (e.g., WMAP polarized maps) combined with existing ones (e.g., Archeops and Boomerang polarization maps) will enable one to do so.

The primordial B -mode signal on large scales (accessible by space-based or balloon-borne experiments) is not contaminated by lensing, but its amplitude is affected by the optical depth to reionization τ . The lensing signal (dominant on scales $\ell \gtrsim 50$) can be removed to high accuracy (delensing) in the absence of noise and foregrounds. Foreground contamination and noise in the foreground templates are the limiting factor in constraining r and in the delensing implementation. For the considered realistic space-based experiments the residual noise (both in the maps and in foreground templates) hinders delensing implementation. Delensing may be used to improve r limits in partial sky ground-based experiments: partial sky experiments can easily achieve lower noise level than space-based ones and can target particularly clean areas of the sky, but accurate foreground templates are still needed to keep foregrounds contamination at or below the 1% level and to reduce template noise.

A space-based or balloon-borne experiment can easily measure $r = 10^{-3}$ (at the ~ 3 - σ level) if foregrounds can be subtracted at 1% level, but foreground contamination is ultimately the limiting factor for a detection of $r \sim 10^{-4}$.

From the ground, $r = 0.01$ can be detected at the 2 - σ level but only if foreground can be subtracted at the 1% level and if accurate foreground templates are available.

In order to have accurate and high resolution foreground templates and for the foregrounds to be subtracted at the percent level, a drastically improved knowledge of the amplitude and the spectral and spatial dependence of polarized foreground emission is needed. This can be achieved by observing the polarized foreground emission on large areas of the sky, at high Galactic latitudes, with high resolution and high sensitivity at multiple wavelengths, both at higher and lower frequencies than the “CMB window”. The success of future B-modes experiments will rely on these efforts. Ongoing and planned experiments such as EBEX, CLOVER, QUaD, Planck, BLASTPol, will play a crucial role in achieving this goal.

If this can be achieved, in order to constrain r as best as possible, a combination of approaches will most likely be needed. A space-based or balloon-borne experiment can be optimized to observe the low ℓ BB “bump”: it can have a wide frequency coverage, but weight restrictions can be met by having less stringent requirements for noise and angular resolution. Future advances to ballooning methods, such as “stratellite”¹² technology may make that avenue particularly attractive. A stratellite has a flight time of 18 months’ duration, is stationed at 65,000 feet and is capable of carrying a payload of up to 3000 lb. In addition the airship is 100% reclaimable and the vehicle will be much cheaper to build and to run than a satellite. These properties may make such an experiment achieve the sky coverage and integration time of a satellite, retaining at the same time the advantages of a balloon-borne experiment (e.g. lower costs, less weight restrictions, upgradable).

A satellite/balloon-borne experiment is nicely complementary to a ground-based partial-sky experiment. The ground-based telescope can be optimized to implement de-lensing: it can observe a particularly clean patch of the sky; and can achieve low noise level by using large detectors arrays. Thus the noise and beam size requirements need to be more stringent than for a full sky experiment tailored to access the reionization bump, and the frequency coverage must be wide enough to still enable accurate (percent level) foreground subtraction.

6.2 Implications for Inflation

What can experiments with the capabilities illustrated here tell us about inflationary physics? Figures 1 and 2 show that, to produce a clearly detectable (>3 - σ) tensor component in any foreseeable CMB experiment, inflation must necessarily involve large-field variations: $\Delta\phi \gtrsim 1$. As Efstathiou & Mack (2005) point out, the relation in Eq. 11 is so steep that, to probe models with small field variations where an effective field theory description is likely to be

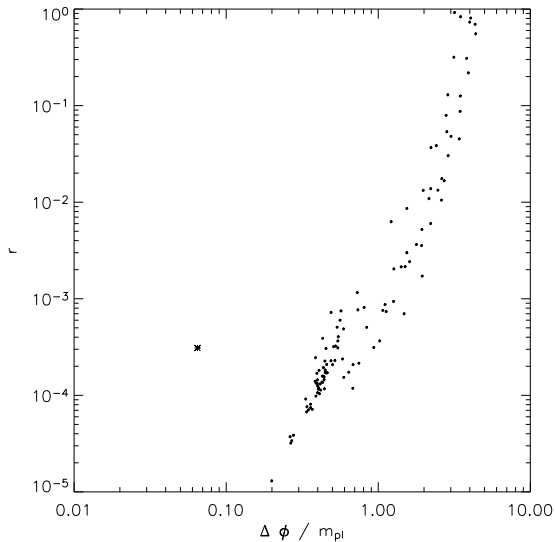


Figure 4. Otherwise identical to Fig. 1 except that the constraints on n_s and $dn_s/d\ln k$ are 2 - σ limits from the CR case of Table 3.

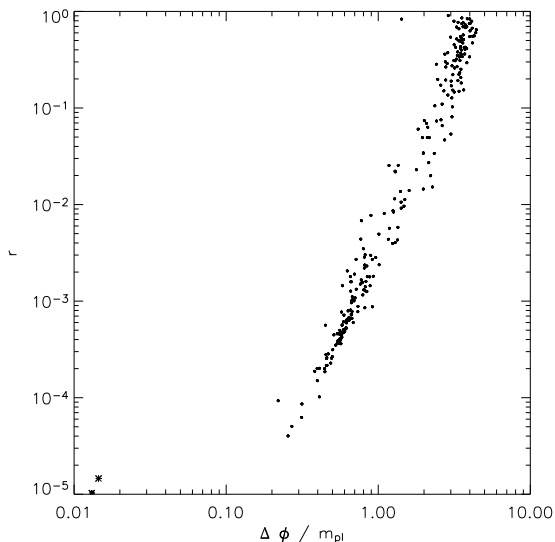


Figure 5. Otherwise identical to Fig. 2 except that the constraints on n_s and $dn_s/d\ln k$ are 2 - σ limits from the CR case of Table 3.

valid, one needs to be able to detect $r \leq 10^{-4}$. This is exceedingly difficult in CMB experiments, given realistic polarized foregrounds, detector noise achievable in the foreseeable future, and the weak lensing contamination of the primordial B -modes. Therefore, in the foreseeable future, it appears that we are limited to testing large-field models of inflation. Figures 4 and 5 show what happens to the $\Delta\phi$ vs. r relation when the observational limits on n_s and $dn_s/d\ln k$ at the level of the 2 - σ limits from the CR case of Table 3 are imposed. Observation of a significant tensor/scalar ratio may therefore be a signal that inflation is being driven by some physics in which the inflaton cannot be described as a fundamental field captured in terms of a low energy effective field theory description such as Eq. 6.

¹² Stratellite: <http://www.sanswire.com>

Note that the converse of this argument is not implied; there are perfectly valid inflation models realized within the effective field theory framework in which the inflaton is not a fundamental field. Alternatively, as Linde (2005) points out, the effective field theory description of $V(\phi)$ becomes invalid only for $V(\phi) > m_{\text{Pl}}^4$, not $\phi > m_{\text{Pl}}$ as inferred from Eq. 6. Chaotic inflation models, such as the simple $\lambda\phi^4$ model (excluded at about the $3\text{-}\sigma$ level by current cosmological constraints), exploit this rationale; on the other hand, building realistic particle-physics motivated chaotic inflation models has historically proved difficult. However, it has been shown recently that chaotic inflation models can be realized in supergravity models if the potential has a shift symmetry (see Linde (2005) and references therein for a detailed explanation). Thus it might be possible to construct chaotic inflation models motivated by realistic particle physics with $\Delta\phi \gtrsim 1$. Further, as Boyanovsky D., de Vega H. L. & Sanchez N. G. (2005) point out, inflation can be described as a series expansion in terms of a new variable $\chi = \phi/(\sqrt{N}m_{\text{Pl}})$, which makes the effective field theory description valid up to $r \sim 1$. In this case ϕ is not a fundamental field but a degree of freedom in the theory.

It is therefore important to investigate the possibility of constructing particle-physics motivated inflationary models with $\Delta\phi \gtrsim 1$, since these are likely to be the only models that could be probed by realistic CMB experiments in the near future. Significant progress in this direction has already been made; for example, extranatural/pseudonatural inflation Hill & Leibovich (2002); Arkani-Hamed et al. (2003a,b), in which the inflaton is the extra component of a gauge field in a 5-dimensional theory compactified in a circle, which predicts a significant production of a tensor component ($r \sim 0.11$). Purely 4d theories appear to require more sophisticated structures in order to protect the flatness of the potential from excessive radiative corrections (Kim et al. 2005; Arkani-Hamed et al. 2003b), and in general do not predict significant gravity-wave production. However they still appear to preserve the prediction of a significant deviation from scale invariance as a signature of inflation.

Conversely, if tensor modes are not detected in these experiments, we can exclude large-field models as a mechanism for inflation. Then we would need to examine the remaining possibilities by investigating constraints on the deviation from scale-invariance of the scalar spectral index (a blue or red index discriminates between classes of inflationary models), and also from its running. While this paper focuses on the implications of a primordial B -mode measurement from foreseeable CMB experiments for inflation, a negligible primordial tensor component is also a prediction of the Ekpyrotic/Cyclic scenarios (Khoury et al. 2002, 2001).

6.3 “Bang for your bucks”

To conclude, in Figure 6 we summarize the minimum experimental set up and foreground knowledge that is needed to measure a given r value at $\gtrsim 3\text{-}\sigma$ level. We also indicate whether the signal comes from the reionization “bump” region (affected by τ) or the “first peak” region (affected by lensing contamination) and if delensing can be used to improve signal to noise. Finally we label the experiments with letters a for ground based, b for balloon-borne and c for

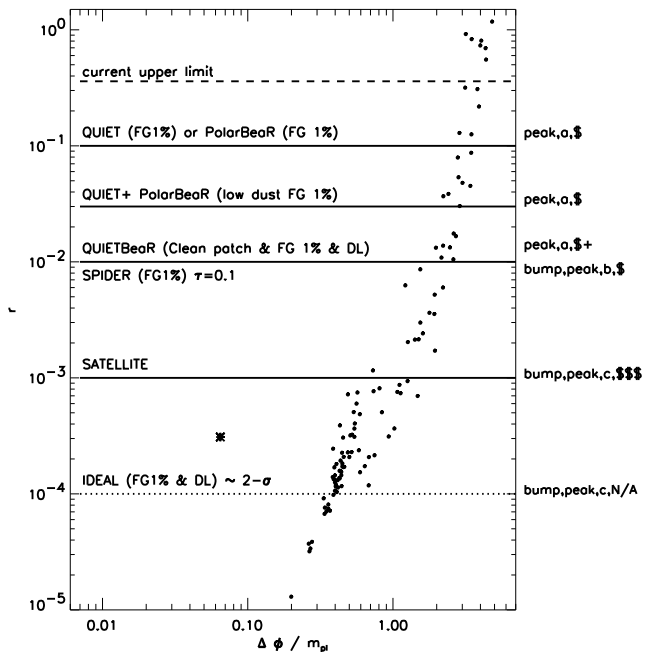


Figure 6. Superimposed upon the Monte-Carlo points of Fig. 4 are the minimum values of r that can be measured at the $3\text{-}\sigma$ level for different experimental setups and foreground knowledge. The legend on the right indicates whether the signal comes from the “peak” ($\ell > 30$) region or the “bump” ($\ell < 30$) region; if the experiment is ground-based (a), balloon-borne (b) or satellite (c); and how expensive such an experiment may be. The top dashed line shows the current upper limit. Single ground-based experiments can reach $r = 0.1$ if foreground subtraction can be done at the 1% level. The signal in this case would come from the peak region and the noise characteristic would not allow delensing. If two different experiments such as QUIET and PolarBeaR can *i*) overlap their survey region and *ii*) select a sky patch with realistic synchrotron contamination (50% of DASI upper limit) and low polarized dust emission (1% of Archeops limit) and *iii*) clean foregrounds to the 1% level, the wider frequency coverage and the lower noise means that $r = 0.03$ can be reached. Also, in this case the signal comes from the peak region. $r = 0.01$ can be reached in two different ways. The technologies of QUIET and PolarBeaR could be combined: QUIET noise properties can be extended to also include PolarBeaR channels, a smaller region of the sky is scanned so that the noise per pixel can be reduced and delensing can be implemented; and the sky region chosen is particularly clean (dust: 1% of Archeops limit; synchrotron: 10% of DASI limit). The signal would come from the “peak” and the measurement would rely on delensing. Alternatively a long duration balloon flight with the specifications of SPIDER would measure the same r but accessing the reionization bump region and without relying on delensing. $r = 10^{-3}$ can be achieved only with a satellite mission. Finally, foreground contamination, even if at the 1% level, is the limiting factor for accessing $r = 10^{-4}$ with an ideal, space based, noiseless experiment.

satellite. These could also be interpreted as price-tags from least expensive (a) to most expensive (c). There is a clear correlation between cost of the experiment and models that can be accessed by it.

ACKNOWLEDGMENTS

We thank Mark Devlin, George Efstathiou, Chao-Lin Kuo, Stephan Meyer, Lyman Page, John Ruhl, Dorothea Samtleben, Kendrick Smith, David Spergel, Huan Tran, Ben Wandelt, and Bruce Winstein for useful conversations, and Eiichiro Komatsu and Adrian Lee for comments on an early version of the manuscript. LV is supported by NASA grant ADP03-0000-0092 and ADP04-0000-0093. HVP is supported by NASA through Hubble Fellowship grant #HF-01177.01-A awarded by the Space Telescope Science Institute, which is operated by the Association of Universities for Research in Astronomy, Inc., for NASA, under contract NAS 5-26555. She acknowledges the hospitality of the Kavli Institute for Particle Astrophysics and Cosmology at Stanford University, where part of this work was carried out. The research of RJ is partially supported by NSF grant AST-0206031.

REFERENCES

- Albrecht A., Steinhardt P. J., 1982, *Physical Review Letters*, 48, 1220
- Arkani-Hamed N., Cheng H. C., Creminelli P., Randall L., 2003a, *Physical Review D*, 90, 221302
- Arkani-Hamed N., Cheng H. C., Creminelli P., Randall L., 2003b, *JCAP*, 0307, 003
- Baccigalupi et al.C., *A&A* 372, 8
- Baccigalupi et al.C., 2004, *MNRAS*, 354, 55
- Bardeen J. M., Steinhardt P. J., Turner M. S., 1983, *PRD*, 28, 679
- Barger V., Lee H., Marfatia D., 2003, *Physics Letters B*, 565, 33
- Bennett et al. 2003a, *ApJS*, 148, 1
- Bennett et al. C. L., 2003b, *ApJS*, 148, 97
- Benoît et al. 2004, *Astron. & Astrophys.*, 424, 571
- Bernardi G., Carretti E., Fabbri R., Sbarra C., Poppi S., Cortiglioni S., 2003, *MNRAS*, 344, 347
- Bernardi G., Carretti E., Fabbri R., Sbarra C., Poppi S., Cortiglioni S., Jonas J. L., 2004, *MNRAS*, 351, 436
- Bond J. R., Jaffe A. H., Knox L., 2000, *ApJ*, 533, 19
- Bowden M., et al., 2004, *MNRAS*, 349, 321
- Boyanovsky D., de Vega H. L. & Sanchez N. G., 2005, *astro-ph/0507595*
- Bruscoli M., Tucci M., Natale V., Carretti E., Fabbri R., Sbarra C., Cortiglioni S., 2002, *New Astronomy*, 7, 171
- Carretti E., Bernardi G., Sault R. J., Cortiglioni S., Poppi S., 2005, *MNRAS*, 358, 1
- Carretti E., McConnell D., McClure-Griffiths N. M., Bernardi G., Cortiglioni S., Poppi S., 2005, *astro-ph/0503043*
- Church et al. S., 2003, *New Astronomy Review*, 47, 1083
- Copeland E. J., Kolb E. W., Liddle A. R., Lidsey J. E., 1993a, *Physical Review Letters*, 71, 219
- Copeland E. J., Kolb E. W., Liddle A. R., Lidsey J. E., 1993b, *PRD*, 48, 2529
- de Oliveira-Costa A., Tegmark M., O'dell C., Keating B., Timbie P., Efstathiou G., Smoot G., 2003, *PRD*, 68, 083003
- Draine B. T., Lazarian A., 1998, *ApJ(Lett)*, 494, L19+
- Easther R., Kinney W. H., 2003, *PRD*, 67, 043511
- Efstathiou G., Mack K. J., 2005, *astro-ph/0503360*
- Finkbeiner D. P., Davis M., Schlegel D. J., 1999, *ApJ*, 524, 867
- Finkbeiner D. P., Langston G. I., Minter A. H., 2004, *ApJ*, 617, 350
- Fisher R. A., 1935, *J. Roy. Stat. Soc.*, 98, 39
- Fosalba P., Lazarian A., Prunet S., Tauber J. A., 2002, *ApJ*, 564, 762
- Giardino G., Banday A. J., Górski K. M., Bennett K., Jonas J. L., Tauber J., 2002, *A&A*, 387, 82
- Guth A. H., 1981, *PRD*, 23, 347
- Guth A. H., Pi S.-Y., 1982, *Physical Review Letters*, 49, 1110
- Hawking S. W., 1982, *Physics Letters B*, 115, 295
- Hill C. T., Leibovich A. K., 2002, *Physical Review D*, 66, 075010
- Hirata C. M., Seljak U., 2003, *PRD*, 68, 083002
- Hoffman M. B., Turner M. S., 2001, *PRD*, 64, 023506
- Hu W., Hedman M. M., Zaldarriaga M., 2003, *PRD*, 67, 043004
- Hu W., Okamoto T., 2002, *ApJ*, 574, 566
- Kamionkowski M., Kosowsky A., Stebbins A., 1997, *Physical Review Letters*, 78, 2058
- Kesden M., Cooray A., Kamionkowski M., 2002, *PRL*, 89, 011304
- Kesden M., Cooray A., Kamionkowski M., 2003, *PRD*, 67, 123507
- Khoury J., Ovrut B. A., Seiberg N., Steinhardt P. J., Turok N., 2002, *Phys. Rev.*, D65, 086007
- Khoury J., Ovrut B. A., Steinhardt P. J., Turok N., 2001, *Phys. Rev.*, D64, 123522
- Kim J. E., Nilles H. P., Peloso M., 2005, *JCAP*, 0501, 005
- Kinney W. H., 2002, *PRD*, 66, 083508
- Kinney W. H., 2003, *New Astronomy Review*, 47, 967
- Kinney W. H., Kolb E. W., Melchiorri A., Riotto A., 2004, *PRD*, 69, 103516
- Knox L., Song Y., 2002, *PRL*, 89, 011303
- Lazarian A., Finkbeiner D., 2003, *New Astronomy Review*, 47, 1107
- Lazarian A., Prunet S., 2002, in *AIP Conf. Proc. 609: Astrophysical Polarized Backgrounds Polarized microwave emission from dust.* pp 32–43
- Leach S. M., Liddle A. R., 2003, *PRD*, 68, 123508
- Leitch E. M., Kovac J. M., Halverson N. W., Carlstrom J. E., Pryke C., Smith M. W. E., 2005, *ApJ*, 624, 10
- Lewis A., Challinor a., Turok N., 2002 *Phys.Rev. D*, 65, 023505
- Liddle A. R., 1994, *PRD*, 49, 739
- Liddle A. R., Leach S. M., 2003, *PRD*, 68, 103503
- Liddle A. R., Lyth D. H., 1993, *Physics Reports*, 231, 1
- Linde A., 2005, *Phys.Scripta*, T117, 40
- Linde A. D., 1982, *Physics Letters B*, 108, 389
- Linde A. D., 1994, *Phys. Rev.*, D49, 748
- Lyth D. H., 1984, *Physics Letters B*, 147, 403
- Lyth D. H., 1997, *Physical Review Letters*, 78, 1861
- Mukhanov V. F., Chibisov G. V., 1981, *ZhETF Pis ma Redaktsiiu*, 33, 549
- Mukhanov V. F., Feldman H. A., Brandenberger R. H., 1992, *Physics Reports*, 215, 203
- Okamoto T., Hu W., 2003, *PRD*, 67, 083002
- Oxley P. et al, 2005, *astro-ph/0501111*
- Padoan P., Goodman A., Draine B. T., Juvela M., Nordlund Å., Röngrvaldsson Ö. E., 2001, *ApJ*, 559, 1005

- Peiris H. V., Komatsu E., Verde L., Spergel D. N., Bennett C. L., Halpern M., Hinshaw G., Jarosik N., Kogut A., Limon M., Meyer S. S., Page L., Tucker G. S., Wollack E., Wright E. L., 2003, *ApJS*, 148, 213
- Platania P., Bensadoun M., Bersanelli M., de Amici G., Kogut A., Levin S., Maino D., Smoot G. F., 1998, *ApJ*, 505, 473
- Platania P., Burigana C., Maino D., Caserini E., Bersanelli M., Cappellini B., Mennella A., 2003, *A&A*, 410, 847
- Prunet S., Sethi S. K., Bouchet F. R., Miville-Deschenes M.-A., 1998, *Astron. & Astrophys.*, 339, 187
- Sato K., 1981, *MNRAS*, 195, 467
- Seljak U., et al., 2004, *astro-ph/0407372*
- Seljak U., Hirata C. M., 2004, *PRD*, 69, 043005
- Seljak U., McDonald P., Makarov A., 2003, *MNRAS*, 342, L79
- Sigurdson K., Cooray A., 2005, *astro-ph/0502549*
- Song Y., Knox L., 2003, *PRD*, 68, 043518
- Spergel D. N., Verde L., Peiris H. V., Komatsu E., Nolte M. R., Bennett C. L., Halpern M., Hinshaw G., Jarosik N., Kogut A., Limon M., Meyer S. S., Page L., Tucker G. S., Weiland J. L., Wollack E., Wright E. L., 2003, *ApJS*, 148, 175
- Spergel D. N., Zaldarriaga M., 1997, *Physical Review Letters*, 79, 2180
- Starobinsky A. A., 1982, *Physics Letters B*, 117, 175
- Stivoli et al., 2005, *astro-ph/0505381*
- Tegmark M., Eisenstein D. J., Hu W., de Oliveira-Costa A., 2000, *ApJ*, 530, 133
- Tucci M., Carretti E., Cecchini S., Nicastro L., Fabbri R., Gaensler B. M., Dickey J. M., McClure-Griffiths N. M., 2002, *ApJ*, 579, 607
- Tucci M., Martinez-Gonzalez E., Vielva P., Delabrouille J., 2004, *MNRAS*, 360, 926
- Tucci M., Martinez-Gonzalez E., Toffolatti L., Gonzalez-Nuevo J., DeZotti G., 2004, *MNRAS*, 349, 1267
- Zaldarriaga M., Seljak U., 1997, *PRD*, 55, 1830
- Zaldarriaga M., Seljak U., 1998, *PRD*, 58, 023003

APPENDIX

Table 6. Constraints on all parameters. IDEAL denotes an ideal experiment (no foregrounds, cosmic variance dominated). SAT denotes a space-based experiment. CR means that the consistency relation for n_T , $n_t = -r/8$ has been imposed. FLT means that flatness has been imposed, this does not affect the errors on the parameters relevant to inflation. FG denotes that galactic foregrounds has been considered. FG1% means that their residual contamination is reduced to 1% while FG10% means that foreground contamination has been reduced to 10%. The experimental specifications used for obtaining these constraints are reported in Table 7. The error on the amplitude does not include possible calibration errors which are likely to dominate. These forecasts have been computed for a fiducial value of $\tau = 0.164$ except where explicitly specified. As the BB signal on large scales is boosted by τ roughly as τ^2 , lower values of τ will degrade the significance of these forecasts. For fiducial τ one sigma below the best fit value the detectability of $r = 0.01$ ($r = 0.03$) from $\ell < 20$ is equivalent to the detectability of $r = 0.03$ ($r = 0.1$) in the best fit model. This consideration affects only large sky coverage experiments which probe the “reionization bump” in the BB spectrum at $\ell < 10$ and does not affect the smaller scale ground-based experiments.

r	case	Δr	Δn	Δn_t	$\Delta dn/d \ln k$	ΔZ	$\Delta \omega_b$	$\Delta \omega_c$	Δh	$\Delta \Omega_K$	Δ_A
0.01		0.001	0.0017	0.056	0.0034	0.0033	6×10^{-5}	0.00027	0.003	0.0006	0.004
0.03	IDEAL	0.0028	0.0017	0.047	0.0036	0.0034	6.4×10^{-5}	0.00026	0.0033	0.0006	0.004
0.1		0.0063	0.0018	0.035	0.0035	0.0036	6×10^{-5}	0.00020	0.0023	0.0006	0.004
0.01		0.00045	0.0017	–	0.0036	0.0032	6.1×10^{-5}	0.00025	0.003	0.0006	0.0038
0.03	IDEAL,	0.00074	0.0017	–	0.0036	0.0032	6.4×10^{-5}	0.00026	0.0032	0.00060	0.0038
0.1	CR	0.0015	0.0017	–	0.0036	0.0032	6.4×10^{-5}	0.00026	0.0024	0.0006	0.0038
0.01	IDEAL	0.000021	0.0021	0.0019	0.0038	0.0038	6.5×10^{-5}	0.00072	0.0057	0.0006	0.0048
0.03	DL	0.000063	0.0021	0.0019	0.0038	0.0038	6.5×10^{-5}	0.00072	0.0057	0.0006	0.0049
0.01	IDEAL	0.000016	0.0021	–	0.0038	0.0038	6.5×10^{-5}	0.00072	0.0057	0.0006	0.0048
0.03	DL CR	0.000049	0.0021	–	0.0038	0.0038	6.4×10^{-5}	0.00072	0.0057	0.0006	0.0049
0.01		0.0030	0.0023	0.098	0.0046	0.0053	8.4×10^{-5}	0.00053	0.0055	0.00078	0.0066
0.03	SAT	0.0048	0.0023	0.069	0.0046	0.0053	8.4×10^{-5}	0.00054	0.0056	0.00080	0.0066
0.1		0.010	0.0023	0.056	0.0046	0.0055	8.4×10^{-5}	0.00055	0.0058	0.00082	0.0068
0.01	SAT	0.0030	0.0023	0.096	0.0046	0.0049	8.3×10^{-5}	0.00050	0.0023	–	0.0062
0.03		0.0047	0.0023	0.068	0.0046	0.0050	8.3×10^{-5}	0.00051	0.0023	–	0.0062
0.1	FLT	0.010	0.0023	0.054	0.0046	0.0050	8.3×10^{-5}	0.00052	0.0023	–	0.0062
0.01		0.0011	0.0023	–	0.0046	0.0052	8.3×10^{-5}	0.00051	0.0054	0.00078	0.0065
0.03	SAT	0.0017	0.0023	–	0.0046	0.0050	8.3×10^{-5}	0.00051	0.0054	0.00078	0.0063
0.1	CR	0.0028	0.0023	–	0.0046	0.0049	8.2×10^{-5}	0.00051	0.0054	0.00080	0.0062
0.01	SAT	0.0031	0.0023	0.098	0.0046	0.0049	8.3×10^{-5}	0.0005	0.0024	–	0.0063
	FG1% FLT										
0.01	+CR	0.001	0.0022	–	0.0046	0.0049	8.3×10^{-5}	0.0005	0.0023	–	0.0062
0.01	SAT,	0.0030	0.0021	0.1	0.0044	0.0040	7.6×10^{-5}	0.00047	0.0021	–	0.0045
	DASI50%, $\tau = 0.1$										
	FG1% FLT										
0.01	+CR	0.0012	0.0020	–	0.0043	0.040	7.6×10^{-5}	0.00046	0.0020	–	0.0045
0.0001	SAT FLT	0.00019	0.0023	0.43	0.0046	0.005	8.3×10^{-5}	0.00051	0.0023	–	0.0063
0.001	FG1% DASI50%	0.0013	0.0023	0.31	0.0046	0.005	8.3×10^{-5}	0.0005	0.0023	–	0.0063
0.0001	SAT FLT CR	0.00012	0.0023	–	0.0046	0.005	8.3×10^{-5}	0.0005	0.0023	–	0.0063
0.001	FG1% DASI50%	0.0003	0.0023	–	0.0046	0.005	8.3×10^{-5}	0.0005	0.0023	–	0.0063
0.01	SAT	0.0035	0.0023	0.11	0.0046	0.005	8.3×10^{-5}	0.00052	0.0024	–	0.0063
	FG10% FLT										
0.01	+CR	0.0013	0.0023	–	0.0046	0.0049	8.3×10^{-5}	0.0005	0.0023	–	0.0063
0.001	SAT FLT	0.00051	0.0023	0.13	0.0046	0.0050	8.3×10^{-5}	0.00051	0.0023	–	0.0063
	FG 10% DASI50%										
0.001	SAT FLT CR	0.00042	0.0023	–	0.0046	0.0050	8.3×10^{-5}	0.00051	0.0023	–	0.0063
	FG 10% DASI50%										
0.0001	SAT NO NOISE										
	FG1% FLT	0.00007	0.0019	0.17	0.0037	0.005	7.4×10^{-5}	0.0022	0.0008	–	0.005
	DASI 50%										
0.0001	+CR	0.000057	0.0019	–	0.0037	0.005	7.4×10^{-5}	0.0022	0.0008	–	0.005

r	case	Δr	Δn	Δn_t	$\Delta dn/d \ln k$	ΔZ	$\Delta \omega_b$	$\Delta \omega_c$	Δh	$\Delta \Omega_K$	Δ_A
0.01	QUIET	0.09	0.029	4.2	0.047	0.06	0.0007	0.005	0.026	–	0.083
0.03	FG1%	0.31	0.03	4.	0.048	0.062	0.0007	0.005	0.025	–	0.083
0.1	FLT	0.32	0.03	1.3	0.48	0.062	0.0007	0.005	0.025	–	0.083
0.01	QUIET	0.015	0.029	–	0.045	0.061	0.00071	0.005	0.024	–	0.08
0.03	FG1% FLT	0.019	0.03	–	0.045	0.062	0.0072	0.005	0.025	–	0.08
0.1	CR	0.035	0.03	–	0.046	0.062	0.00072	0.005	0.024	–	0.08
0.01	QUIET	0.13	0.03	6.0	0.047	0.063	0.0007	0.005	0.023	–	0.08
0.03	FG 10%	0.32	0.032	5.1	0.05	0.063	0.0007	0.05	0.025	–	0.08
0.1	FLT	0.35	0.032	1.4	0.05	0.063	0.0007	0.005	0.024	–	0.08
0.01	QUIET	0.019	0.03	–	0.047	0.06	0.0007	0.005	0.023	–	0.08
0.03	FG10%,FLT	0.024	0.047	–	0.047	0.06	0.0007	0.005	0.023	–	0.08
0.1	CR	0.037	0.024	–	0.046	0.06	0.0007	0.005	0.023	–	0.08
0.01	PolarBeaR	0.07	0.018	3.7	0.037	0.049	0.0006	0.0043	0.018	–	0.06
0.03	DASI50%, Dust1%	0.1	0.018	2.1	0.037	0.051	0.00062	0.0044	0.019	–	0.06
0.1	FG1% FLT	0.1	0.018	0.59	0.037	0.052	0.00062	0.0044	0.019	–	0.06
0.01	PolarBeaR	0.012	0.018	–	0.037	0.051	0.00061	0.0043	0.019	–	0.06
0.03	DASI50%, dust1%	0.015	0.018	–	0.037	0.051	0.00061	0.0043	0.019	–	0.06
0.1	FG1% FLT CR	0.023	0.018	–	0.037	0.052	0.00061	0.0043	0.019	–	0.06
0.01	QUIET+PolarBeaR	0.036	0.017	2.0	0.033	0.058	0.00066	0.0046	0.02	–	0.067
0.03	DASI50%dust1%	0.08	0.02	1.7	0.039	0.063	0.00067	0.0049	0.021	–	0.067
0.1	FLT FG 1%	0.08	0.02	0.47	0.039	0.06	0.00064	0.0047	0.02	–	0.067
0.01	QUIET+PolarBeaR	0.006	0.015	–	0.03	0.058	0.00066	0.0046	0.02	–	0.067
0.03	DASI50%dust1%	0.009	0.02	–	0.039	0.063	0.00067	0.0048	0.021	–	0.067
0.1	FLT FG 1% CR	0.017	0.02	–	0.039	0.06	0.00064	0.0046	0.02	–	0.067
0.01	QUIETBeaR										
0.01	DASI10%, dust1%	0.017	0.054	1.0	0.094	0.15	0.0016	0.01	0.05	–	0.19
0.01	FG 1% FLT +CR	0.003	0.054	–	0.093	0.15	0.0016	0.01	0.05	–	0.19
0.01	SPIDER, $\tau = 0.1$										
0.01	DASI50%	0.02	0.1	0.44	0.06	0.007	0.002	0.01	0.04	–	0.1
0.01	FG 1% FLT +CR	0.004	0.1	–	0.06	0.007	0.002	0.009	0.03	–	0.09

Table 7. Experimental specifications used for computing cosmological constraints.

	frequency (GHz)	noise/beam (μ K)	beam FWHM (')	sky coverage (f_{sky} or sq. deg.)
SAT	30, 50, 70, 100, 200	2.2 per channel	8	$f_{sky}=0.8$
QUIET	40	0.43	23	4×400
	90	0.78	10	
PolarBeaR	90	1.6	6.7	500
	150	2.4	4.0	
	220	11.3	2.7	
QUIET+PolarBeaR	40	0.43	23	400
	90	0.78	10	
	90	1.6	6.7	
	150	2.4	4.0	
	220	11.3	2.7	
QUIETBeaR	40	0.1	23	170
	90	0.18	10	
	90	0.18	10	
	150	0.18	10	
	220	0.18	10	
SPIDER	40	0.74	145	$f_{sky}=0.4$
	84	0.36	69	
	92	0.36	63	
	100	0.36	58	
	145	0.58	40	
	220	1.6	26	